JCI The Journal of Clinical Investigation

Dynamic metabolism of endothelial triglycerides protects against atherosclerosis in mice

Nabil E. Boutagy, … , Carlos Fernandez-Hernando, William C. Sessa

J Clin Invest. 2024. https://doi.org/10.1172/JCI170453.

Research In-Press Preview Vascular biology

Graphical abstract

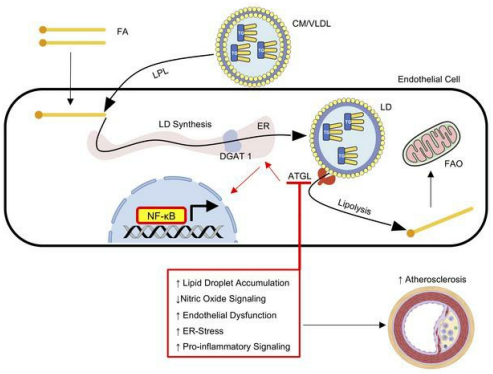

Dynamic metabolism of endothelial triglycerides protects against atherosclerosis in mice

Nabil E. Boutagy[+*1,2], Ana Gamez-Mendez[+1,2], Joseph W Fowler[1,2], Hanming Zhang[2,3], Bal K. Chaube[2,3], Enric Esplugues[2,3], Sungwoon Lee[1,2], Daiki Horikami[1,2], Jiasheng Zhang[5], Kathryn M. Citrin[2,3], Abhishek Singh[1,2], Brian G. Coon[6,7], Yajaira Suarez[2,3,4], Carlos Fernandez-Hernando[2,3,4], and William C. Sessa[1,2,5]

1. Department of Pharmacology, Yale University School of Medicine, New Haven, Connecticut, 06520, USA.
2. Vascular Biology and Therapeutics Program, Yale University School of Medicine, New Haven, Connecticut, 06520, USA.
3. Department of Comparative Medicine, Yale University School of Medicine, New Haven, Connecticut, 06520 USA.
4. Department of Pathology, Yale University School of Medicine, New Haven, Connecticut, 06520 USA.
5. Department of Cardiology, Yale University School of Medicine, New Haven, Connecticut, 06520 USA.
6. Cardiovascular Biology Research Program, Oklahoma Medical Research Foundation, Oklahoma City, OK, 73104 USA.
7. Department of Cell Biology, University of Oklahoma Health Sciences Center, Oklahoma City, OK 73104, USA

[+] NEB and AGM contributed equally to this paper.

***Corresponding author:**

Nabil E. Boutagy, Ph.D. Associate Research Scientist, Vascular Biology & Therapeutics Program, Department of Pharmacology, Yale University School of Medicine, Amistad Research Building, 10 Amistad St, New Haven, CT 06520, USA, Tel: (203)737-2291; Fax: (203)737- 2290; E-mail: nabil.boutagy@yale.edu

Competing interests: WCS is a member of the scientific advisory board of Alucent and Antibe Therapeutics, and the Senior Vice President and Chief Scientific Officer for the Internal Medicine Research Unit at Pfizer.

ABSTRACT

Blood vessels are continually exposed to circulating lipids and elevations of ApoB containing lipoproteins cause atherosclerosis. Lipoprotein metabolism is highly regulated by lipolysis, largely at the level of the capillary endothelium lining metabolically active tissues. How large blood vessels, the site of atherosclerotic vascular disease, regulate the flux of fatty acids (FA) into triglyceride (TG) rich lipid droplets (LD) is not known. In this study, we showed that deletion of the enzyme, adipose triglyceride lipase (ATGL) in the endothelium, led to neutral lipid accumulation in vessels and impaired endothelial dependent vascular tone and nitric oxide synthesis to promote endothelial dysfunction. Mechanistically, the loss of ATGL led to endoplasmic reticulum stress-induced inflammation in the endothelium. Consistent with this mechanism, deletion of endothelial ATGL markedly increased lesion size in a model of atherosclerosis. Together, these data demonstrate that the dynamics of FA flux through LD impacts endothelial cell homeostasis and consequently large vessel function during normal physiology and in a chronic disease state.

INTRODUCTION

The vascular endothelium is essential in lipid partitioning (1). Specifically, in metabolically active tissues (e.g., heart, skeletal muscle, adipose), triglyceride (TG) rich lipoproteins (chylomicrons, V-LDL) are metabolized by lipoprotein lipase (LPL), which docks on the luminal surface of capillaries together with the protein, GPIHBP1 (2). Following lipolysis, FAs traverse the endothelium via passive diffusion (3) or receptor-mediated uptake to be metabolized or stored in underlying parenchymal cells (1). Recent data has shown that receptor mediated uptake of FA by the small vessel endothelium is critical for maintaining metabolic homeostasis, and that the aortic endothelium is capable of endocytosing TG-rich lipoproteins by a receptor mediated, LPL independent process (4-6). However, little is known about how endothelial cells (ECs) process lipids after uptake, especially in large vessels—the site of atherosclerotic vascular disease.

Lipid droplets (LDs) are dynamic intracellular organelles that assemble, store and release lipids depending on energy status of the cell (7). During conditions of energy surplus, cells can esterify free FA into TG for storage in LDs. TG synthesis is an early step in LD biogenesis, a multiple step process that occurs in the endoplasmic reticulum (ER), and is rate limited by diacylglycerol O-acyltransferase enzymes (DGAT-1 and -2) (8). Alternatively, LD components can be liberated by a series of hydrolysis reactions, leading to the production of lipid metabolites that are used for energy provision, membrane synthesis, transcriptional control and/or cell signaling (7). The rate limiting enzyme in LD hydrolysis is adipose triglyceride lipase (ATGL) (also known as patatin-like phospholipase domain-containing protein 2 [PNPLA2]), which is a lipase found on the surface of LDs that together with its coactivator, comparative gene identification-58 (CGI58), catalyzes the initial step in TG lipolysis (9, 10).

The essential role of ATGL in LD metabolism and human physiology was uncovered by several clinical case reports describing mutations in the *ATGL* and *CGI58* genes (11). Mutations in these genes cause neutral lipid storage disease (NLSD), an autosomal recessive disorder

characterized by excessive TG accumulation in multiple tissues (11). Patients with mutations in the *ATGL* gene develop a more severe clinical prognosis, characterized by myopathy (NLSD-M), compared to individuals with mutations in *CGI58* that develop NLSD with Ichthyosis (NLSD-I)(12). Individuals with NLSD-M accumulate TG rich LDs in the liver, skeletal muscle, and heart, which are associated with elevated liver enzymes, muscle weakness and systolic dysfunction. Detailed analysis of an explanted heart from a patient with a homozygous loss of function mutation in exon 7 of *ATGL* (c.865C →T; p.Gln289X) revealed unusual atherosclerotic plaques characterized by massive neutral lipid accumulation in endothelial and smooth muscle cells and medial thickening of the coronary vessel wall (13). Several other patients with loss of function mutations in *ATGL* display this phenotype, defined as primary triglyceride deposit cardiomyovasculopathy (14, 15), suggesting that ATGL-dependent lipolysis regulates TG hydrolysis in large blood vessels.

Impaired ATGL mediated LD hydrolysis influences whole-body metabolism and systemic tissue function (9, 16). For example, transgenic mice with adipose specific ATGL deletion display a marked reduction in adipose lipolysis, which leads to protection from diet induced insulin resistance (17), but an impairment in acute exercise performance (18). In addition, mice with a global deletion of ATGL present a severe phenotype characterized by premature death caused by extensive lipid accumulation and defective ß-oxidation in cardiac tissue (16). Interestingly, global ATGL deficient mice exhibit endothelial dysfunction in the macro- and microvasculature, which is partially linked to a reduction in LD derived ligands of peroxisome proliferator receptor alpha (PPARα) signaling, as well as marked perivascular fat inflammation (19). Despite the extensive characterization of ATGL mediated control of lipid metabolism in cardiac and adipose tissue, the cell autonomous role of ATGL in EC lipid metabolism and function is poorly understood.

Recent data from our group has shown that ECs contain the machinery for LD formation and metabolism in micro- and macrovascular ECs (20). In vitro, microvascular EC synthesize LD to buffer lipotoxicity, and hydrolyze LD to liberate FA that can be oxidized by the mitochondria or released from cells for delivery to parenchymal cells (20). LD hydrolysis in these cells is rate

limited by ATGL and is negatively regulated by CAV-1 (21). Interestingly, LD accumulation was observed in large vessel ECs following postprandial lipid challenge in mice. The presence of neutral lipid pools in the endothelium of mammalian atheromas suggests that endothelial LD accumulation may contribute to large vessel dysfunction (22, 23). Although global *Atgl* knockout mice display endothelial dysfunction, the endothelial cell autonomous role of ATGL and LD accumulation cannot be deciphered using this model due to confounding from marked dysfunction in other tissues that can impair vascular function. Therefore, we generated endothelial-specific *Atgl* knockout mice to systematically explore the function of TG hydrolysis in intact blood vessels.

Here we show that endothelial-specific ATGL ablation leads to neutral lipid accumulation in the endothelium of large vessels and impairs large vessel endothelial dependent vascular tone though a reduction in nitric oxide (NO) synthesis. Using bulk RNA sequencing and several complementary functional read-outs, we demonstrate that the loss of ATGL in endothelial cultures upregulates endoplasmic reticulum (ER) stress, which in turn, heightens pro-inflammatory signaling. Notably, single cell RNA sequencing of aortic ECs validated these findings in vivo. Consistent with this mechanism, deletion of endothelial ATGL markedly increases lesion size in a murine model of atherosclerosis. Together, these data demonstrate that the dynamics of FA flux through LD impacts EC homeostasis and consequently large vessel function during normal physiology and in a chronic disease state.

RESULTS

Loss of ATGL in the endothelium leads to spontaneous neutral TG lipid accumulation

EC specific ATGL knockout (*Atgl* ECKO) were mice generated by crossing *Atgl*$^{flox/flox}$ mice with endothelial-specific, *Cdh5*-Cre (VE-cadherin-Cre) transgenic mice. EC specific ATGL deletion was confirmed and *Atgl* mRNA (Fig. 1A) and protein levels (Fig. 1B) were markedly reduced in mouse lung EC (LECs) of *Atgl* ECKO compared to *Atgl*$^{flox/flox}$ (control) littermate mice. Accordingly, the loss of ATGL in LECs enhanced baseline levels of neutral lipids and augmented LD formation by oleic acid (OA) loading as assessed by both the neutral lipid dye, BODIPY 493/503 (Fig. 1C) and direct measurement of TG content (Fig. 1D). In addition to microvascular cells, *Atgl* mRNA was significantly reduced in FACS purified ECs ($CD31^+/CD45^-$) from the aorta of *Atgl* ECKO compared to control mice (Fig. 1E). Consistently, *en face* imaging of BODIPY 493/503 showed that TG rich neutral lipids were detectable in the endothelial layer of abdominal aortas from overnight fasted *Atgl* ECKO mice (Fig. 1F), and this effect was further accentuated by *ex vivo* incubation of the vessel with OA (1 mM). Similarly, *en face* imaging of the lesser curvature of aortic arch, an atherosclerosis prone region of the vessel wall, showed more postprandial TG-rich neutral lipid accumulation in endothelial layer of the aorta in *Atgl* ECKO following an olive oil gavage compared to control mice (Fig. 1G). Thus, the loss of ATGL in the endothelium leads to neutral lipid accumulation in both micro- and macro-vessels. Notably, *Atgl* ECKO mice are viable, gain weight, and display similar levels of fasted glucose and circulating total cholesterol, triglycerides, and non-esterified fatty acids (NEFA) compared control littermates on a standard chow (SC) diet (Supplemental Fig. 1 A-E). In addition, *Atgl* ECKO do not display structural vascular defects as determined by staining the retinal vasculature with isolectin-B4 at P6 (Supplemental Fig. 2). Furthermore, *Atgl* mRNA levels were not different in thioglycollate-elicited peritoneal $CD11b^+$ macrophages between *Atgl* ECKO and control littermates (Supplemental Fig 3).

ATGL ECKO mice have impaired large vessel endothelial-dependent relaxation and reduced nitric oxide synthesis

To examine if the loss of ATGL in EC had any impact on vessel function, we examined vasomotor function of mouse aortic segments using wire myography (24). Phenylephrine (PE) induced tension development was elevated (Fig. 2A), whereas acetylcholine (Ach) induced relaxation (Fig. 2B) was reduced in aortas from *Atgl* ECKO compared to littermate control vessels. However, the direct vasorelaxant actions of sodium nitroprusside (SNP) was not different between the genotypes (Fig. 2C), implying endothelial dysfunction. Since eNOS derived nitric oxide (NO) is the primary vasorelaxing factor produced by large vessel endothelium (25), these data imply that the loss of ATGL impairs eNOS derived NO production. eNOS is abundantly present in a tight perinuclear, Golgi pattern in aortic ECs (26) (Fig. 2D, left panel), and this staining pattern is eliminated in aorta from eNOS KO mice (far right panel). Interestingly, the levels of immunoreactive eNOS were reduced in *Atgl* ECKO aortas compared to control littermates (middle panel and quantified in Fig 2E). The reduction in eNOS levels in *Atgl* ECKO mice was observed throughout several regions of the aorta compared to control mice (Supplemental Fig 4). In addition, eNOS protein levels as determined by Western blotting were significantly reduced in aortic homogenates from *Atgl* ECKO compared to control mice (Fig. 2F and quantified in Fig. 2G). In accordance with reduced eNOS protein levels, the bioavailability of NO, measured as NO bound hemoglobin (NO-Hb) by EPR spectroscopy (24, 27), was significantly reduced in *Atgl* ECKO compared to control mice (Fig. 2H). However, despite these reductions, carotid blood pressure was no different between the genotypes (Supplemental Fig. 5). Thus, the loss of EC ATGL promotes EC dysfunction and reduces NO bioavailability, without influencing systemic blood pressure.

The loss of ATGL in EC induces a pro-inflammatory gene expression profile

To gain mechanistic insights into how the loss of ATGL impacts EC gene expression and subsequent function, total RNA sequencing (RNAseq) was performed in LEC isolated from control and *Atgl* ECKO mice. As displayed by the volcano plot in Fig. 3A, a total of 742 genes were significantly up (n=372) or down (n=370) regulated by the loss of ATGL in LECs. Ingenuity Pathway Analysis demonstrated that the loss of ATGL markedly upregulates several inflammatory signaling pathways (Fig. 3B) and Upstream Regulator Analysis identified that the highest abundance of elevated genes was regulated by the TNF pathway. Consistently, the expression of several proinflammatory genes were significantly upregulated by the loss of ATGL as shown by the heatmap in Fig. 3C. Thus, the loss of ATGL in EC induces a pro-inflammatory phenotype. In independent experiments, RT-qPCR was used to validate RNAseq results. Consistently, basal and TNFα (10 ng/mL, 16 hrs) stimulated mRNA levels of *Vcam1* (vascular cell adhesion molecule 1) and *Ptgs2* (prostaglandin-endoperoxide synthase 2 [encoding COX2]) were significantly higher in *Atgl* ECKO compared to control LECs (Fig. 3D).

The loss of ATGL in EC upregulates VCAM1 surface expression

The induction of endothelial vascular cell adhesion molecule 1 (VCAM1) is tightly regulated by NFκB (28) and is essential for leukocyte binding and subsequent diapedeses into the subendothelial space during inflammation and early atherogenesis (29). Therefore, we used several orthogonal approaches to functionally validate changes in *Vcam1* mRNA. As measured by flow cytometry, *Atgl* ECKO had higher surface levels of VCAM1 under basal (Fig. 3E) and TNFα stimulated conditions (10 ng/mL, 16 hrs) (Fig. 3F) compared to control LECs. Considering that VCAM1 is induced by various inflammatory signals and is dependent on NFκB signaling, control and *Atgl* ECKO LECs were treated overnight with bacterial lipopolysaccharide (LPS, 16h) in the presence or absence of the IκB kinase (IKK) complex inhibitor, BMS-345541 (IKKi). Flow cytometry determined VCAM1 surface levels were significantly higher following LPS activation in

LECs from *Atgl* ECKO compared to control mice and VCAM1 levels were reduced in LECs from both genotypes after IKK inhibition (Fig. 3G). Notably, elevations in VCAM1 in LECs from *Atgl* ECKO were not associated with lung pathology, nor increased neutrophil numbers compared to control mice fed a SC diet (Supplemental Fig 6). Prior work has documented the expression of VCAM1 in the atheroprone, lesser curvature region of the aortic arch in mice fed a SC diet (30). Consistent with in vitro experiments, endothelial loss of ATGL in vivo led to enhanced levels of immunoreactive VCAM1 in the lesser curvature of the aortic arch of *Atgl* ECKO mice compared to control mice (Fig. 3H).

Endoplasmic reticulum stress heightens pro-inflammatory responses in ECs that lack ATGL

Lipid accumulation is associated with endoplasmic reticulum (ER) stress and insulin resistance in metabolic tissues of obese individuals (31, 32). In cultured human EC, lipid induced ER stress partially mediates the induction of several pro-inflammatory chemokines/cytokines (e.g., IL-6, CXCL8, CCL2) (33). Thus, ER stress may mediate the heightened pro-inflammatory signaling observed in ECs that lack ATGL. To test this hypothesis, RNAseq was used to identify significantly different ER stress genes between control and *Atgl* ECKO ECs. As shown in Fig. 4A, several ER stress genes, including *Atf4*, *Ddit3* (encodes CHOP), *Ppp1r15a* (encodes GADD34), and *Ero1l* were upregulated in *Atgl* ECKO compared to control ECs. Conversely, the ER stress genes, *Hspa5, Xbp1,* and *Hsp90b1* were not different between the genotypes. Next, control and *Atgl* ECKO ECs were subjected to palmitate dosing to functionally assess ER stress. Interestingly, both ATF4 and CHOP protein levels were significantly higher at baseline in *Atgl* ECKO compared to control LECs (Fig 4B and quantified in Fig 4E-F), and these elevations coincided with higher protein levels of VCAM1 and COX2 (Fig 4B and quantified in Fig 4C-D). In addition, *Atgl* ECKO had a substantial left shift in inflammatory and ER stress responses to palmitate loading (16 hrs), as evidenced by significantly greater protein levels of VCAM1, COX2, ATF4 and CHOP at lower

doses of palmitate compared to control LECs (Fig 4B and quantified in Fig 4C-F). Next, sodium 4-phenylbutyrate (4-PBA), a chemical chaperone that buffers protein aggregates and ER stress (34), was used to further dissect the relationship between ER stress and pro-inflammatory signaling in EC with ATGL deletion. In vehicle treated cells, 4-PBA significantly reduced ATF4 and CHOP, as well VCAM1, protein levels in *Atgl* ECKO ECs (Fig 4G, and quantified in Fig 4H, J-K). In addition, pretreatment with 4-PBA significantly rescued the heightened VCAM1, COX2, ATF4, and CHOP induction in response to palmitate (0.1 mM, 16 hrs) in *Atgl* ECKO LECs (Fig 4G, and quantified in Fig 4H, J-K). As palmitate leads to cell stress and pro-inflammatory signaling via multiple pathways, we aimed to isolate pro-inflammatory signaling with the use of TNFα. Consistent with palmitate loading, pretreatment with 4-PBA was able to completely rescue heightened surface levels of VCAM1 in TNFα (10 ng/mL, 16 hrs) stimulated conditions in *Atgl* ECKO LECs (Fig 4L-M). Taken together, these data suggest loss of ATGL in EC induces ER stress, which at least in part, contributes to heightened pro-inflammatory signaling at baseline and in response to several inflammatory stimuli.

Endothelial deficiency of ATGL accelerates atherosclerosis

ER-stress related gene expression, including, *ATF4* and *CHOP* mRNA levels, are elevated in the endothelium of coronary artery regions that are prone to atherosclerosis versus regions that resistant to atherosclerosis (35). In addition, protein levels of ATF4 are upregulated in inflamed endothelium of human atherosclerotic lesions (33). Therefore, the upregulation of ER stress and pro-inflammatory signaling in the endothelium of animals that lack ATGL may accelerate atherosclerosis. Thus, to test the EC autonomous role of ATGL during atherosclerosis, congenic *Atgl* ECKO mice were bred to *Apoe* deficient mice (ApoE$^{-/-}$) and fed an atherogenic diet (40% Kcal from Fat + 1.25% Cholesterol) for 12 weeks. *Atgl* ECKO/ApoE$^{-/-}$ mice gained weight similarly to controls (*Atgl*$^{f/f}$/ApoE$^{-/-}$, Supplemental Fig. 7A), displayed similar elevations in total

cholesterol (Supplemental Fig. 7B), but had slightly reduced levels of TG (Supplemental Fig. 7C). *En face* imaging of neutral lipid accumulation using Oil Red O demonstrated a marked increase in aortic lesion size in *Atgl* ECKO/ApoE$^{-/-}$ mice compared to littermate controls (Fig. 5A and quantified in 5B). Similarly, increases in lesion size were observed in several vessel segments, including the roots of the aortic sinus (Fig. 5C and quantified in 5E) and brachiocephalic arteries (BCA; Fig. 5D and quantified in F). Serial analysis of the BCA determined greater global lesion development throughout the entire length of vessels from *Atgl* ECKO/ApoE$^{-/-}$ compared to control mice (Supplemental Fig. 8A and quantified in 8B). In line with endothelial activation (29), analysis of macrophage content showed greater CD68 positive macrophages in aortic root lesions of *Atgl* ECKO/ApoE$^{-/-}$ mice compared to control mice. Thus, the loss of ATGL in EC accelerates atherosclerosis.

Endothelial deficiency of ATGL upregulates ER-stress and pro-inflammatory gene expression in aortic endothelial cells prior to overt plaque development

Endothelial activation is an early process in atherosclerotic progression (36, 37). As plaques develop, intimal immune cells can further activate the endothelium by secreting a myriad of pro-inflammatory mediators (38). Therefore, to translate mechanistic findings in LECs, while avoiding confounding from macrophage laden lesions in *Atgl* ECKO mice, we injected control and *Atgl* ECKO mice with a recombinant adeno-associated virus encoding a constituently active gain of function form of murine PCSK9 (rAAV8-*mPcsk9*) and subjected these mice to short-term atherogenic feeding (4-weeks) to allow for a more gradual progression of atherosclerotic lesions compared to ApoE$^{-/-}$ mice. Control + *mPcsk9* and *Atgl* ECKO + *mPcsk9* had similar body weight and circulating total cholesterol levels following short-term atherogenic diet feeding (Supplemental 9 Fig. A-B). In addition, plaque sizes were small in the aortic sinus and were no different between the genotypes following 4-weeks of atherogenic diet feeding (Supplemental 9 Fig. C). To investigate the molecular and cellular signature of aortic ECs that lack ATGL during

the early stages of atherosclerosis progression, single cell RNA sequencing (scRNA-seq) was performed on cells isolated of aortae from control + *mPcsk9* and *Atgl* ECKO + *mPcsk9* mice after 4-weeks of atherogenic diet feeding (n=4/group). The analysis identified 6 distinct cell clusters based on gene expression patterns of canonical markers of fibroblasts, smooth muscle cells (SMCs), red blood cells (RBCs), endothelial cells (ECs) and CD45+ immune cells (Fig. 6A-B). Next, differential gene expression (DGE) was performed on the EC cluster (Fig. 6C) and analyzed by ingenuity pathway analysis (IPA). Pathway enrichment analysis identified that pathways involved in ER-stress (EIF2 signaling and unfolded protein response) and pro-inflammatory signaling (IL-17A signaling) were highly upregulated in aortic EC from *Atgl* ECKO + *mPcsk9* compared to control + *mPcsk9* mice fed an atherogenic diet for 4-weeks (Fig. 6D). Other interesting, upregulated pathways in aortic ECs from *Atgl* ECKO + *mPcsk9* were the CLEAR (Coordinated Lysosomal Expression and Regulation) and Microautophagy signaling pathways, which may be compensatory mechanisms to degrade accumulating LDs upon loss of ATGL (39). In line with in vitro studies in LECs, expression profiles in aortic ECs from *Atgl* + *mPcsk9* showed higher expression of *Hspa5* (encodes BiP*), Ddit3* (encodes CHOP*), Atf4,* and *Vcam1* compared to control + *mPcsk9* mice fed an atherogenic diet for 4-weeks (Fig. 6E). To functionally confirm some of these changes, FACS was used to measure VCAM1 surface expression levels in aortic ECs ($CD31^+/CD45^-$) from control + *mPcsk9* and *Atgl* ECKO + *mPcsk9* mice fed an atherogenic diet for 4-weeks. Consistent with scRNAseq data, VCAM1 levels were significantly higher in aortic ECs from *Atgl* ECKO + *mPcsk9* compared to control + *mPcsk9* mice fed an atherogenic diet for 4-weeks (Fig. 6F). Together, these data bolster our mechanistic findings in LECs, and suggest that the loss of ATGL in the endothelium upregulates ER-stress and pro-inflammatory signaling pathways, and that these changes occur prior to overt plaque development.

DISCUSSION

Under physiological conditions, the large vessel endothelium can transiently form and degrade TG-rich LDs in response to a lipid challenge (6, 20). The presence LDs in the endothelium of mammalian atheromas suggests that endothelial LD accumulation may contribute to large vessel dysfunction (22, 23). The key salient finding in this study is the demonstration that endothelial-specific ATGL ablation leads to neutral lipid accumulation in the entire vascular tree, promotes endothelial dysfunction, and accelerates atherosclerosis in a murine disease model. Mechanistically, the loss of endothelial ATGL leads to ER stress-induced inflammation, which is characterized by the upregulation of numerous pro-inflammatory genes that are associated with endothelial dysfunction and atherosclerosis (29, 40). Together, these data show that the dynamics of FA flux through LD impacts EC homeostasis in normal blood vessels and alterations in TG hydrolysis, here initiated by the EC loss of ATGL, impedes EC quiescence to promote EC dysfunction and vascular disease in the absence of changing plasma lipids. As such, dissecting the mechanisms that regulate FA flux and LD metabolism in large vessel EC may lead to a deeper understanding of how circulating lipids impact cardiovascular disease.

Despite optimal cholesterol lowering with statins and other cholesterol-lowering strategies, some individuals still experience a high-risk of atherosclerotic incidents due, in part, to persistently elevated TG-rich lipoproteins (41-44). Despite epidemiological evidence indicating circulating TG-rich lipoproteins as independent predictors of cardiovascular and all-cause mortality, the precise mechanisms mediating TG-rich lipoproteins processing in large vessels are unclear, and thus, how to therapeutically target these lipoproteins for risk reduction are poorly defined (44, 45). In our previous studies, we demonstrated that the aortic endothelium has the capability to synthesize and degrade LDs following a lipid challenge (20). Here, we extend these findings and show that deletion of the enzyme, ATGL, in the endothelium leads to neutral lipid accumulation in large vessels and impairs endothelial dependent vascular tone and NO synthesis to promote endothelial dysfunction and atherosclerosis (discussed below). Interestingly, recent studies by

Cabodevilla et al. showed that the aortic endothelium is capable of endocytosing TG-rich lipoproteins by a receptor mediated process (6). Taken together, these studies provide unique insights into how large vessel endothelium, the site of atherosclerotic disease, process TG rich lipoprotein/lipids to maintain EC homeostasis and function during normal physiology and in a chronic disease state.

Under normal conditions, the endothelium regulates vascular homeostasis by modulating vascular tone, maintaining blood fluidity and flow, controlling vessel-wall permeability, and mitigating vascular inflammation (46), and these actions are largely mediated by eNOS derived NO (25). As such, a reduction in bioactive NO due to decreased eNOS activity, eNOS uncoupling, and/or a decline in eNOS protein levels is associated with endothelial dysfunction, hypertension, atherosclerosis, coronary artery disease, and heart failure (37, 47). In this study, we show that mice with endothelial specific deletion of ATGL have a reduction in eNOS protein levels along the length mice of the aorta, alerted endothelial-dependent vasomotor function, and consistently, have a reduction in circulating levels of NO compared to control mice. These findings are in line with a previous report that demonstrated a reduction in aortic eNOS protein levels and altered endothelial-dependent vasomotor function in aortic rings in mice with global deletion of ATGL compared to control mice (19). Indeed, our results clarify the endothelial specific role of TG hydrolysis in the regulation of eNOS, as mice with global deletion of ATGL have markedly enlarged and inflamed perivascular fat surrounding the aorta, reduced cardiac output, and reduced levels of PPARα ligands—all of which can influence NO synthesis (48-50). Despite the reduction in bioactive NO, blood pressure was not elevated in *Atgl* ECKO compared to control mice on a standard chow diet. In the current study, eNOS protein levels were reduced by ~50% in *Atgl* ECKO compared to control mice, which is similar to reductions observed in mice heterozygous for the *Nos3* gene that also display normal blood pressure (51). In contrast to our findings, a recent study showed that endothelial ATGL deletion leads to a reduction in eNOS protein levels by ~40%, which are sufficient to modestly (~10%) elevate systolic blood pressure

compared to control mice (52).The reasons for the discrepancy between our findings are unclear but may be due to the source of *Atgl*$^{flox/flox}$ mice, the extent of *Atgl* excision and/or differences in blood pressure acquisition techniques.

The reduction in eNOS in *Atgl* ECKO mice suggested heightened endothelial pro-inflammatory signaling since inflammatory cytokines (e.g., TNFα, INFγ, CRP) have been demonstrated to potently decrease eNOS levels through several mechanisms (53-57). Consistent with this supposition, deletion of endothelial ATGL was associated with heightened endothelial inflammation. Specifically, whole transcriptome sequencing and pathway analysis revealed that the baseline transcript level of several chemokines/cytokines (e.g., *Ccl2*, *Cxcl5*, *Cxcl12, Ptgs2*) and adhesion molecules (*Vcam1*) were upregulated in LECs that lack ATGL. Notably, mice with endothelial ATGL deletion had higher baseline levels of VCAM1 expression in athero-prone regions of the aortic arch, and ECs from lungs of *Atgl* ECKO animals had higher levels of VCAM1 surface expression and COX-2 protein levels at baseline and in response to several pro-inflammatory stimuli. These mechanistic findings in LECs are in line with studies in human EC cultures that demonstrate elevated TNFα induction of ICAM1 (intracellular adhesion molecule 1) and NFκB signaling following siRNA mediated knockdown of *ATGL* (58). In addition, ECs from aorta of *Atgl* ECKO mice injected with *mPcsk9* and fed an atherogenic diet for four weeks showed elevated endothelial pro-inflammatory transcripts and VCAM1 surface expression levels prior to plaque development compared to control mice. Consistent with elevated endothelial activation (29), *Atgl* ECKO/ApoE$^{-/-}$ mice developed significantly larger atherosclerotic lesions in large vessels compared to ApoE$^{-/-}$ mice. Interestingly, the relationship between ATGL and pro-inflammatory signaling seems to be dependent on cell/tissue type and disease context. For example, a recent study demonstrated that downregulation of *ATGL* in LPS-stimulated macrophages attenuated IL-6 and prostaglandin-E2 production (59). These effects were attributed to reduced availability of LD derived eicosanoids, as ATGL hydrolysis of TGs has been demonstrated to liberate esterified arachidonic acid in immune and other cell types (60, 61).

These recent findings may partially explain the smaller atherosclerotic lesions in LDL receptor knockout mice that were transplanted with bone marrow from global *Atgl* knockout mice (62). Interestingly, the metabolic actions of ATGL in metabolic tissues complicate the relationship between ATGL and inflammation in vivo, as evidenced in adipose specific *Atgl* knockout mice that have reduced immune cell infiltration and improved insulin signaling in the liver (likely due to less adipose FA delivery), but greater pro-inflammatory gene expression and immune cell infiltration in adipose tissue in response to high fat diet induced obesity (17). Nevertheless, our data clearly indicates that the loss of ATGL heightens pro-inflammatory signaling in the endothelium, which in turn, hastens the progression of atherosclerosis. A recent study confirmed the link between endothelial ATGL, pro-inflammatory signaling, and eNOS levels, since silencing of the NFκB subunit, *RELA*, rescued the reduction of eNOS levels observed in ECs with depleted ATGL (52). Interestingly, ATGL silencing and LD accumulation in HUVEC can lead to sequestration of *NOS3* mRNA stabilizing proteins (i.e., PCBP1) and consequent *NOS3* mRNA destabilization (52). Therefore, endothelial ATGL can regulate eNOS levels via both pro-inflammatory signaling dependent and independent pathways.

Previous studies in human ECs showed that the ER stress mediators, ATF4 and XBP1, strongly regulated the induction of several chemokines/cytokines in response to oxidized 1-palmitoyl-2-arachidonyl-*sn*-3-glycero-phosphorylcholine and tunicamycin (33). Using a series of complementary experiments, we demonstrate that loss of endothelial ATGL upregulates basal and palmitate induced ER stress, and that inhibition of ER stress with the chemical chaperones, 4-PBA, largely abrogated heightened proinflammatory signaling in LECs that lack ATGL. In addition, using scRNAseq, we demonstrated that ER-stress and unfolded protein response pathways are upregulated in aortic ECs of *Atgl* ECKO mice injected with *mPcsk9* and fed an atherogenic diet for four weeks compared to control mice, and that these changes occur prior to plaque development. The finding that ATGL deletion upregulates ER-stress is somewhat surprising in the context of our and others previous findings that show that TG synthesis, primarily

through the actions of DGAT1, buffers against lipid-induced ER-stress (20, 63). Rather than being contradictory, our combined results suppose a complex biology in which TG synthesis attenuates lipid-induced ER-stress by esterifying toxic lipid intermediates, whereas impaired TG clearance upregulates ER-stress though other stress signaling pathways. In macrophages, *Atgl* deletion upregulates ER-stress (64) and this is postulated to occur through impaired mitochondrial function and $Ca2^{+}$ signaling (65). We and other have previously reported that FA derived from ATGL hydrolysis provide substrate for mitochondrial ß-oxidation (16, 20). Recent studies in ECs underscore the importance of ß-oxidation in maintaining redox balance and endothelium quiescence (66). Thus, it is possible that oxidative stress, secondary to impaired TG hydrolysis, mediates ER-stress in ECs that lack ATGL. However, precisely how ATGL deletion upregulates ER stress in ECs is unknown and mechanistic and metabolic trace studies are needed to parse out these mechanisms.

In summary, endothelial specific deletion of the rate limiting enzyme of TG-hydrolysis, ATGL, leads to neutral lipid accumulation in the vascular tree, promotes endothelial dysfunction, and accelerates atherosclerosis in a murine disease model. Mechanistically, the loss of ATGL causes ER-stress- induced endothelial activation through NFκB signaling. Collectively, the results from these integrated experiments provide insights into how alterations in endothelial LD dynamics impact vascular function in health and disease.

METHODS

Endothelial-specific adipose triglyceride lipase knockout (*Atgl* ECKO) mice were generated by crossbreeding *Atgl*$^{flox/flox}$ mice (B6N.129-Pnpla2tm1Eek/J) with *Cdh5*-Cre transgenic mice (B6.FVB-Tg [*Cdh5*-cre]7Mlia/J). *Atgl* ECKO were injected with recombinant adeno-associated virus 8 (rAAV8) encoding constitutively active murine PCSK9 ([rAAV8-*mPcsk9*], $1*10^{11}$ vg) for short-term atherosclerosis studies (4-weeks) or were crossed with ApoE null mice (ApoE $^{-/-}$) to generate *Atgl* ECKO/ApoE$^{-/-}$ mice for long-term atherosclerosis studies (12-weeks). For these studies, atherosclerosis was accelerated by feeding mice with an atherogenic diet (40% Kcal from fat + 1.25% cholesterol, Research Diets, D12108). Mice were subjected to a wide range of techniques to comprehensively investigate the role of endothelial ATGL in various physiological and pathological processes, including, single cell RNA sequencing (scRNAseq) (GSE246138), *en face* immunostaining of aortae, in vivo olive oil challenge, ex vivo vascular reactivity of aortae, whole blood assessment of nitric oxide bioavailability, and blood pressure measurements. Mouse lung endothelial cells were cultured from *Atgl* ECKO mice for RNA sequencing (GSE246083), western blotting, immunostaining, and FACS to investigate cellular and molecular consequences of ATGL deletion from the endothelium. Statistical analyses were performed using Prism 9 software, with significance set at $P < 0.05$. All animal procedures were performed under protocols reviewed and approved by Yale University (New Haven, CT) Institutional Animal Care and Use Committee. Expanded methods are provided in the supplemental materials.

Author Contributions NB, AGM, and WCS conceived the project, designed experiments, and wrote the manuscript. JWF performed RNAseq analysis, assisted with mechanistic studies, analyzed data, and edited the manuscript. HZ performed scRNAseq acquisition and analysis, assisted with in vivo studies and edited the manuscript. EE performed FACS analysis of aorta for VCAM1 assisted in experimental design. SL performed retina isolation and staining. DH assisted in vivo studies and blindly performed lung tissue processing pathology. AK performed early work in vivo, and isolated and characterized LEC, and assisted in experimental design. JZ performed the blood pressure measurements and assisted with analysis. KMC assisted with in vivo experiments and contributed to data analysis. BKC and YS provided conceptual insight towards mechanistic experiments, helped analyze data, and edited the manuscript. AS, HZ, KMC, and CFH assisted with atherosclerosis studies, helped analyzed the data, and edited the manuscript. BGC assisted with experiments, provided key conceptual insight towards mechanistic experiments, helped analyze data and edited the manuscript. WCS supervised the project.

Acknowledgements. This work was supported by NIH grant R35HL139945, R01DK125492 and an American Heart Association MERIT Award (WCS) and K01DK124441 (NEB).

References:

1. Boutagy NE, Singh AK, and Sessa WC. Targeting the vasculature in cardiometabolic disease. *Journal of Clinical Investigation.* 2022;132(6):e148556.
2. Young SG, Song W, Yang Y, Birrane G, Jiang H, Beigneux AP, et al. A protein of capillary endothelial cells, GPIHBP1, is crucial for plasma triglyceride metabolism. *Proceedings of the National Academy of Sciences.* 2022;119(36):e2211136119.
3. He C, Weston TA, Jung RS, Heizer P, Larsson M, Hu X, et al. NanoSIMS analysis of intravascular lipolysis and lipid movement across capillaries and into cardiomyocytes. *Cell metabolism.* 2018;27(5):1055-66. e3.
4. Son N-H, Basu D, Samovski D, Pietka TA, Peche VS, Willecke F, et al. Endothelial cell CD36 optimizes tissue fatty acid uptake. *Journal of Clinical Investigation.* 2018;128(10):4329-42.
5. Hagberg CE, Falkevall A, Wang X, Larsson E, Huusko J, Nilsson I, et al. Vascular endothelial growth factor B controls endothelial fatty acid uptake. *Nature.* 2010;464(7290):917.
6. Cabodevilla AG, Tang S, Lee S, Mullick AE, Aleman JO, Hussain MM, et al. Eruptive xanthoma model reveals endothelial cells internalize and metabolize chylomicrons, leading to extravascular triglyceride accumulation. *The Journal of Clinical Investigation.* 2021;131(12).
7. Walther TC, and Farese Jr RV. Lipid droplets and cellular lipid metabolism. *Annual review of biochemistry.* 2012;81:687-714.
8. Harris CA, Haas JT, Streeper RS, Stone SJ, Kumari M, Yang K, et al. DGAT enzymes are required for triacylglycerol synthesis and lipid droplets in adipocytes [S]. *Journal of lipid research.* 2011;52(4):657-67.
9. Zimmermann R, Strauss JG, Haemmerle G, Schoiswohl G, Birner-Gruenberger R, Riederer M, et al. Fat mobilization in adipose tissue is promoted by adipose triglyceride lipase. *Science.* 2004;306(5700):1383-6.
10. Lass A, Zimmermann R, Haemmerle G, Riederer M, Schoiswohl G, Schweiger M, et al. Adipose triglyceride lipase-mediated lipolysis of cellular fat stores is activated by CGI-58 and defective in Chanarin-Dorfman Syndrome. *Cell metabolism.* 2006;3(5):309-19.
11. Schweiger M, Lass A, Zimmermann R, Eichmann TO, and Zechner R. Neutral lipid storage disease: genetic disorders caused by mutations in adipose triglyceride lipase/PNPLA2 or CGI-58/ABHD5. *American journal of physiology-endocrinology and metabolism.* 2009;297(2):E289-E96.
12. Fischer J, Lefèvre C, Morava E, Mussini J-M, Laforêt P, Negre-Salvayre A, et al. The gene encoding adipose triglyceride lipase (PNPLA2) is mutated in neutral lipid storage disease with myopathy. *Nature genetics.* 2007;39(1):28-30.
13. Hirano K-i, Ikeda Y, Zaima N, Sakata Y, and Matsumiya G. Triglyceride deposit cardiomyovasculopathy. *New England Journal of Medicine.* 2008;359(22):2396-8.

14. Li M, Hirano K-i, Ikeda Y, Higashi M, Hashimoto C, Zhang B, et al. Triglyceride deposit cardiomyovasculopathy: a rare cardiovascular disorder. *Orphanet journal of rare diseases.* 2019;14(1):1-9.
15. Onishi T, Nakano Y, Hirano K-i, Nagasawa Y, Niwa T, Tajima A, et al. Prevalence and clinical outcomes of triglyceride deposit cardiomyovasculopathy among haemodialysis patients. *Heart.* 2021;107(2):127-34.
16. Haemmerle G, Moustafa T, Woelkart G, Buttner S, Schmidt A, van de Weijer T, et al. ATGL-mediated fat catabolism regulates cardiac mitochondrial function via PPAR-alpha and PGC-1. *Nat Med.* 2011;17(9):1076-85.
17. Schoiswohl G, Stefanovic-Racic M, Menke MN, Wills RC, Surlow BA, Basantani MK, et al. Impact of reduced ATGL-mediated adipocyte lipolysis on obesity-associated insulin resistance and inflammation in male mice. *Endocrinology.* 2015;156(10):3610-24.
18. Dubé JJ, Sitnick MT, Schoiswohl G, Wills RC, Basantani MK, Cai L, et al. Adipose triglyceride lipase deletion from adipocytes, but not skeletal myocytes, impairs acute exercise performance in mice. *American Journal of Physiology-Endocrinology and Metabolism.* 2015;308(10):E879-E90.
19. Schrammel A, Mussbacher M, Wölkart G, Stessel H, Pail K, Winkler S, et al. Endothelial dysfunction in adipose triglyceride lipase deficiency. *Biochimica et Biophysica Acta (BBA)-Molecular and Cell Biology of Lipids.* 2014;1841(6):906-17.
20. Kuo A, Lee MY, and Sessa WC. Lipid droplet biogenesis and function in the endothelium. *Circulation research.* 2017;120(8):1289-97.
21. Kuo A, Lee MY, Yang K, Gross RW, and Sessa WC. Caveolin-1 regulates lipid droplet metabolism in endothelial cells via autocrine prostacyclin-stimulated, cAMP-mediated lipolysis. *J Biol Chem.* 2018;293(3):973-83.
22. Simionescu M. Implications of early structural-functional changes in the endothelium for vascular disease. *Arteriosclerosis, thrombosis, and vascular biology.* 2007;27(2):266-74.
23. Guyton J, and Klemp K. Early extracellular and cellular lipid deposits in aorta of cholesterol-fed rabbits. *The American journal of pathology.* 1992;141(4):925.
24. Lee MY, Gamez-Mendez A, Zhang J, Zhuang Z, Vinyard DJ, Kraehling J, et al. Endothelial cell autonomous role of Akt1: regulation of vascular tone and ischemia-induced arteriogenesis. *Arteriosclerosis, thrombosis, and vascular biology.* 2018;38(4):870-9.
25. Forstermann U, and Sessa WC. Nitric oxide synthases: regulation and function. *Eur Heart J.* 2012;33(7):829-37, 37a-37d.
26. Sessa WC, Garca-Cardea G, Liu J, Keh A, Pollock JS, Bradley J, et al. The Golgi Association of Endothelial Nitric Oxide Synthase Is Necessary for the Efficient Synthesis of Nitric Oxide (∗). *Journal of Biological Chemistry.* 1995;270(30):17641-4.
27. Kraehling JR, Hao Z, Lee MY, Vinyard DJ, Velazquez H, Liu X, et al. Uncoupling Caveolae From Intracellular Signaling In Vivo. *Circ Res.* 2016;118(1):48-55.
28. Iademarco M, McQuillan JJ, Rosen G, and Dean D. Characterization of the promoter for vascular cell adhesion molecule-1 (VCAM-1). *Journal of Biological Chemistry.* 1992;267(23):16323-9.
29. Cybulsky MI, Iiyama K, Li H, Zhu S, Chen M, Iiyama M, et al. A major role for VCAM-1, but not ICAM-1, in early atherosclerosis. *The Journal of clinical investigation.* 2001;107(10):1255-62.

30. Iiyama K, Hajra L, Iiyama M, Li H, DiChiara M, Medoff BD, et al. Patterns of vascular cell adhesion molecule-1 and intercellular adhesion molecule-1 expression in rabbit and mouse atherosclerotic lesions and at sites predisposed to lesion formation. *Circulation research.* 1999;85(2):199-207.
31. Gregor MF, Yang L, Fabbrini E, Mohammed BS, Eagon JC, Hotamisligil GS, et al. Endoplasmic reticulum stress is reduced in tissues of obese subjects after weight loss. *Diabetes.* 2009;58(3):693-700.
32. Boden G, Duan X, Homko C, Molina EJ, Song W, Perez O, et al. Increase in endoplasmic reticulum stress–related proteins and genes in adipose tissue of obese, insulin-resistant individuals. *Diabetes.* 2008;57(9):2438-44.
33. Gargalovic PS, Gharavi NM, Clark MJ, Pagnon J, Yang W-P, He A, et al. The unfolded protein response is an important regulator of inflammatory genes in endothelial cells. *Arteriosclerosis, thrombosis, and vascular biology.* 2006;26(11):2490-6.
34. Cortez L, and Sim V. The therapeutic potential of chemical chaperones in protein folding diseases. *Prion.* 2014;8(2):197-202.
35. Civelek M, Manduchi E, Riley RJ, Stoeckert Jr CJ, and Davies PF. Chronic endoplasmic reticulum stress activates unfolded protein response in arterial endothelium in regions of susceptibility to atherosclerosis. *Circulation research.* 2009;105(5):453-61.
36. Pober JS, and Sessa WC. Evolving functions of endothelial cells in inflammation. *Nature Reviews Immunology.* 2007;7(10):803-15.
37. Widlansky ME, Gokce N, Keaney JF, and Vita JA. The clinical implications of endothelial dysfunction. *Journal of the American College of Cardiology.* 2003;42(7):1149-60.
38. Gimbrone Jr MA, and García-Cardeña G. Endothelial cell dysfunction and the pathobiology of atherosclerosis. *Circulation research.* 2016;118(4):620-36.
39. Schulze RJ, Krueger EW, Weller SG, Johnson KM, Casey CA, Schott MB, et al. Direct lysosome-based autophagy of lipid droplets in hepatocytes. *Proceedings of the National Academy of Sciences.* 2020;117(51):32443-52.
40. Winter C, Silvestre-Roig C, Ortega-Gomez A, Lemnitzer P, Poelman H, Schumski A, et al. Chrono-pharmacological targeting of the CCL2-CCR2 axis ameliorates atherosclerosis. *Cell metabolism.* 2018;28(1):175-82. e5.
41. Matsuura Y, Kanter JE, and Bornfeldt KE. Highlighting residual atherosclerotic cardiovascular disease risk. *Arteriosclerosis, thrombosis, and vascular biology.* 2019;39(1):e1-e9.
42. Tall AR, Thomas DG, Gonzalez-Cabodevilla AG, and Goldberg IJ. Addressing dyslipidemic risk beyond LDL-cholesterol. *The Journal of clinical investigation.* 2022;132(1).
43. Nordestgaard BG. Triglyceride-rich lipoproteins and atherosclerotic cardiovascular disease: new insights from epidemiology, genetics, and biology. *Circulation research.* 2016;118(4):547-63.
44. Bhatt DL, Steg PG, Miller M, Brinton EA, Jacobson TA, Ketchum SB, et al. Cardiovascular risk reduction with icosapent ethyl for hypertriglyceridemia. *New England Journal of Medicine.* 2019;380(1):11-22.
45. Nicholls SJ, Lincoff AM, Garcia M, Bash D, Ballantyne CM, Barter PJ, et al. Effect of high-dose omega-3 fatty acids vs corn oil on major adverse cardiovascular events in

patients at high cardiovascular risk: the STRENGTH randomized clinical trial. *Jama.* 2020;324(22):2268-80.
46. Winkler G, Lakatos P, Salamon F, Nagy Z, Speer G, Kovacs M, et al. Elevated serum TNF-α level as a link between endothelial dysfunction and insulin resistance in normotensive obese patients. *Diabetic Medicine.* 1999;16(3):207-11.
47. Massion P, Feron O, Dessy C, and Balligand J-L. Nitric oxide and cardiac function: ten years after, and continuing. *Circulation research.* 2003;93(5):388-98.
48. Craige SM, Kröller-Schön S, Li C, Kant S, Cai S, Chen K, et al. PGC-1α dictates endothelial function through regulation of eNOS expression. *Scientific reports.* 2016;6:38210.
49. Smith CJ, Sun D, Hoegler C, Roth BS, Zhang X, Zhao G, et al. Reduced gene expression of vascular endothelial NO synthase and cyclooxygenase-1 in heart failure. *Circulation research.* 1996;78(1):58-64.
50. Marchesi C, Ebrahimian T, Angulo O, Paradis P, and Schiffrin EL. Endothelial nitric oxide synthase uncoupling and perivascular adipose oxidative stress and inflammation contribute to vascular dysfunction in a rodent model of metabolic syndrome. *Hypertension.* 2009;54(6):1384-92.
51. Shesely EG, Maeda N, Kim H-S, Desai KM, Krege JH, Laubach VE, et al. Elevated blood pressures in mice lacking endothelial nitric oxide synthase. *Proceedings of the National Academy of Sciences.* 1996;93(23):13176-81.
52. Kim B, Zhao W, Tang SY, Levin MG, Ibrahim A, Yang Y, et al. Endothelial lipid droplets suppress eNOS to link high fat consumption to blood pressure elevation. *The Journal of Clinical Investigation.* 2023.
53. Venugopal SK, Devaraj S, Yuhanna I, Shaul P, and Jialal I. Demonstration that C-reactive protein decreases eNOS expression and bioactivity in human aortic endothelial cells. *Circulation.* 2002;106(12):1439-41.
54. Koh KP, Wang Y, Yi T, Shiao SL, Lorber MI, Sessa WC, et al. T cell-mediated vascular dysfunction of human allografts results from IFN-gamma dysregulation of NO synthase. *J Clin Invest.* 2004;114(6):846-56.
55. Yan G, You B, Chen SP, Liao JK, and Sun J. Tumor necrosis factor-alpha downregulates endothelial nitric oxide synthase mRNA stability via translation elongation factor 1-alpha 1. *Circ Res.* 2008;103(6):591-7.
56. Hu S, Pi Q, Luo M, Cheng Z, Liang X, Luo S, et al. Contribution of the NLRP3/IL-1beta axis to impaired vasodilation in sepsis through facilitation of eNOS proteolysis and the protective role of melatonin. *Int Immunopharmacol.* 2021;93:107388.
57. Nigro P, Abe J-i, Woo C-H, Satoh K, McClain C, O'Dell MR, et al. PKCζ decreases eNOS protein stability via inhibitory phosphorylation of ERK5. *Blood, The Journal of the American Society of Hematology.* 2010;116(11):1971-9.
58. Inoue T, Kobayashi K, Inoguchi T, Sonoda N, Fujii M, Maeda Y, et al. Reduced expression of adipose triglyceride lipase enhances tumor necrosis factor α-induced intercellular adhesion molecule-1 expression in human aortic endothelial cells via protein kinase C-dependent activation of nuclear factor-κB. *Journal of Biological Chemistry.* 2011;286(37):32045-53.
59. van Dierendonck XA, Vrieling F, Smeehuijzen L, Deng L, Boogaard JP, Croes C-A, et al. Triglyceride breakdown from lipid droplets regulates the inflammatory response in

macrophages. *Proceedings of the National Academy of Sciences.* 2022;119(12):e2114739119.
60. Dichlberger A, Schlager S, Maaninka K, Schneider WJ, and Kovanen PT. Adipose triglyceride lipase regulates eicosanoid production in activated human mast cells. *Journal of lipid research.* 2014;55(12):2471-8.
61. Riederer M, Lechleitner M, Köfeler H, and Frank S. Reduced expression of adipose triglyceride lipase decreases arachidonic acid release and prostacyclin secretion in human aortic endothelial cells. *Archives of physiology and biochemistry.* 2017;123(4):249-53.
62. Lammers B, Chandak PG, Aflaki E, Van Puijvelde GH, Radovic B, Hildebrand RB, et al. Macrophage adipose triglyceride lipase deficiency attenuates atherosclerotic lesion development in low-density lipoprotein receptor knockout mice. *Arteriosclerosis, thrombosis, and vascular biology.* 2011;31(1):67-73.
63. Chitraju C, Mejhert N, Haas JT, Diaz-Ramirez LG, Grueter CA, Imbriglio JE, et al. Triglyceride synthesis by DGAT1 protects adipocytes from lipid-induced ER stress during lipolysis. *Cell metabolism.* 2017;26(2):407-18. e3.
64. Aflaki E, Doddapattar P, Radović B, Povoden S, Kolb D, Vujić N, et al. C16 ceramide is crucial for triacylglycerol-induced apoptosis in macrophages. *Cell death & disease.* 2012;3(3):e280-e.
65. Aflaki E, Radović B, Chandak PG, Kolb D, Eisenberg T, Ring J, et al. Triacylglycerol accumulation activates the mitochondrial apoptosis pathway in macrophages. *Journal of Biological Chemistry.* 2011;286(9):7418-28.
66. Kalucka J, Bierhansl L, Conchinha NV, Missiaen R, Elia I, Brüning U, et al. Quiescent endothelial cells upregulate fatty acid β-oxidation for vasculoprotection via redox homeostasis. *Cell metabolism.* 2018;28(6):881-94. e13.

Figure Legends:

Figure 1. Loss of endothelial-specific ATGL leads to spontaneous vascular lipid droplet accumulation in vivo and ex vivo. (A) qRT-PCR analysis of *Atgl* mRNA in lung endothelial cells (LEC) from control and *Atgl* ECKO mice (n=3/group) ****p<0.0001, unpaired two-tailed Student's t-test. **(B)** Representative Western Blot analysis showing ATGL protein levels in LEC isolated from control and *Atgl* ECKO mice (Each replicate is from 3 independent experiments) **(C)** Representative confocal fluorescence images of lipid droplet (LD) detected with BODIPY 493/503 (green) in cultured LEC in EGM-2 media supplemented with either vehicle (-OA) or 1 mM OA (oleic acid) overnight. Hoechst 33342 (blue) was used for nuclei staining. **D)** Corresponding triglyceride (TG) levels quantified in cell lysates (n=3-4/group) *p<0.01, **p=0.003, ***p=0.0001, One-way ANOVA with Tukey's post-test. Scale bar,10 μm**. (E)** qRT-PCR analysis of *Atgl* mRNA in FACS purified aortic endothelial cells ($CD31^+/CD45^-$) from control and *Atgl* ECKO mice (n=3/group) ***p<0.001, unpaired two-tailed Student's t-test. **(F)** En face images of abdominal aorta from fasted control and *Atgl* ECKO mice exposed ex vivo to vehicle (-OA) or 1 mM BSA complexed oleic acid (+OA) in EGM-2 media for 4 hours (n=5 mice/group). The aorta was immunostained for VE-cadherin (VECAD; (red) and LD were stained with BODIPY 493/503 (green). Scale bar, 25 μm. **(G)** En face images of LD formed in ascending aorta (lesser curvature) in vivo 3h after an olive oil oral gavage (10 mL/kg) in control (left panel) and *Atgl* ECKO mice (far right panel). LD were detected using BODIPY 493/503 and endothelial cells were detected by immunostaining for VECAD. The middle panel is a schematic drawing that illustrates the area analyzed (n=3/group). Scale bar, 75μm. All data represent the mean ± SEM**.**

Figure 2. ATGL deficiency leads to endothelial dysfunction. (A) Cumulative concentration-response curves of developed isometric tension in response to phenylephrine (PE) in aortic rings harvested from control and *Atgl* ECKO mice. **(B)** Cumulative concentration-response curves representing percent relaxation of pre-contracted vessels in response to acetylcholine (ACh) and **(C)** the $NO^{\cdot}$ donor, sodium nitroprusside (SNP), in aortic rings harvested from control and *Atgl* ECKO mice. Results represent mean values ± SEM of 5-6 individual experiments (4 rings per mouse) **p*<0.05, Two-way ANOVA with a Sidak's multiple comparison test. **(D)** Representative confocal images of en face immunostaining of eNOS protein levels (yellow) in thoracic aorta from control (far left), *Atgl* ECKO (middle panel) and $eNOS^{-/-}$ (far right) mice processed and stained identically. Endothelial cells were detected by immunostaining for VECAD (red), and nuclei were stained with DAPI (blue). **(E)** Quantification of aortic images (n=3/group) ***p*<0.01, unpaired two-tailed Student's t-test. Scale bar, 50 μm. **(F)** Representative Western Blot analysis showing eNOS protein levels in aortic homogenates of control and *Atgl* ECKO mice and **G)** Quantification of (n=6/group) **p*<0.05, unpaired two-tailed Student's t-test. **H)** Electron paramagnetic resonance determined nitrosyl-hemoglobin (NO-Hb) in venous blood as an index of NO bioavailability in control and *Atgl* ECKO mice. (n=6/group) **p*<0.05, unpaired two-tailed Student's t-test.

Figure 3. Loss of ATGL in the endothelium upregulates pro-inflammatory gene expression and VCAM1 surface levels. **(A)** Volcano plot for differential expression genes (DEGs) from bulk RNA sequencing in lung endothelial cells (LEC) that fall above the threshold values ([log2(FC) -1 or 1 and -log10(pval) > 1.3], red lines) are pictured. Loss of ATGL upregulated 372 genes and downregulated 370 genes in LECs. The red colored dot represents *Pnpla2* (ATGL gene name) for reference. **B)** Canonical Pathway Analysis and Upstream Regulator Analysis (URA) of signaling pathways and gene regulators, respectively, that were significantly higher in *Atgl* ECKO compared to control LECs. **C)** Clustered heatmap from RNA-seq data showing significantly changed DEGs involved in inflammation between control and *Atgl* ECKO LEC (n=3 replicates/group)**. D)** qRT-PCR analysis of *Vcam1* and *Ptgs2* mRNA in lung endothelial cells (LEC) at baseline and treated with mouse TNFα overnight (10 ng/mL,16 hours) from control and *Atgl* ECKO mice (n=3/group). **p<0.01, ***p<0.001, ****p<0.0001, Two-way ANOVA with Siadak's multiple comparison test**. E)** Basal and **F)** TNFα stimulated (10 ng/mL,16 hours) surface VCAM1 levels between control and *Atgl* ECKO LECs (n=4 replicates/group) determined by FACS and PE-VCAM1 (Mean fluorescence intensity, MFI). *****p*<0.0001, unpaired two-tailed Student's t-test. **G)** Surface VCAM1 levels determined by FACS and PE-VCAM1 (MFI) following overnight (16 hrs) lipopolysaccharide (LPS, 1 μg/mL) treatment ± the IκB kinase (IKK) complex inhibitor, BMS-345541 (IKKi, 10 μM, 30-minute pretreatment) in LECs. (n=3 replicates/group). *****p*<0.0001, Two-way ANOVA, Sidak's multiple comparison test. **H)** Representative immunostaining analysis of VCAM1 (green), CD31 (red) and nuclei (DAPI, blue) in the ascending aorta (lesser curvature) from control and *Atgl* ECKO mice after an overnight fast. (n=3/group). L=Lumen. Scale bar, 100 μm.

Figure 4. Loss of endothelial-specific ATGL leads to endoplasmic reticulum (ER) stress-induced inflammation. A) Clustered heatmap from RNA-seq data showing significantly different DEGs involved in endoplasmic reticulum (ER) stress between control and *Atgl* ECKO LEC (n=3 replicates/group). **B)** Representative Western Blot analysis showing higher baseline ER stress marker (ATF4, CHOP) protein levels, as well as heightened ER stress and inflammatory (VCAM1, COX2) responsiveness to palmitate (0-0.25. mM,16 hrs) dosing between control and *Atgl* ECKO LEC. Quantification of VCAM1 **(C),** COX2 **(D)**, CHOP **(E)**, and ATF4 **(F)** from palmitate dosing (n=3 independent experiments). **p*<0.05, ***p*<0.01, *****p*<0.001, Two-way ANOVA, Sidak's multiple comparison test. **G)** Representative Western Blot analysis showing the rescue of baseline VCAM1 and ER stress marker (ATF4, CHOP) levels, as well as the rescue of heightened VCAM1,

COX2, ATF4, and CHOP levels in response to palmitate (100 μM, 16 hrs) in the presence or absence of the global ER stress inhibitor, sodium 4-phenylbutyrate (4-PBA, 2.5 mM, 8-hour pre-treatment) in *Atgl* ECKO LECs. Quantification of VCAM1 **(H)**, COX2 **(I),** CHOP **(J)**, and ATF4 **(K)** from panel G (n=3 independent experiments). **p*<0.05, ***p*<0.01, *****p*<0.001, Two-way ANOVA, Sidak's multiple comparison test. **(L)** Flow cytometry histogram of PE-VCAM1 between control LECs treated with TNFα (solid blue), *Atgl* ECKO LECs treated with TNFα (solid red), control LECs treated with TNFα in the presence of 4-PBA (dashed blue) and *Atgl* ECKO LECs treated with TNFα in the presence of 4-PBA (dashed red). (M) Quantification of mean fluorescent intensity (MFI) of PE-VCAM1 between control and *Atgl* ECKO following overnight (16 hrs) TNFα (10 ng/mL) in the presence or absence of 4-PBA (2.5 mM, 8-hour pre-treatment). (n=4 replicates/group). *****p*<0.0001, Two-way ANOVA, Sidak's multiple comparison test.

Figure 5. Endothelial deficiency of ATGL accelerates atherosclerosis. A) Representative *en face* images of the luminal surface of mouse aorta (aortic root to common iliac bifurcation) stained for Oil Red O (ORO) to delineate lipid-rich lesions between control and *Atgl* ECKO on a ApoE-/- background following 12 weeks of atherogenic diet feeding. **B)** Corresponding quantification of plaque area as a percentage of total aortic luminal area (n=10-12/group). *****p*<0.0001, unpaired two-tailed Student's t-test. **C)** Representative histological staining of aortic sinus stained with ORO and **D)** brachiocephalic artery (BCA) cross-sections stained with ORO and hematoxylin for plaque lesions. Scale bar, 500 μm. **E)** Quantification of the absolute plaque area (n=8-9/group) of lesions present in the aortic root and **F)** BCA (n=8-9/group). *****p*<0.0001, unpaired two-tailed Student's t-test. **G)** Representative immunofluorescence images of aortic sinus cross-sections staining of CD68+ macrophages (red) and smooth muscle α-actin+ (SMC) (green) cells. Nuclei were DAPI-counterstained (blue) (n=5/group). Scale bar, 750 μm. **H)** Bar graph showing quantification of CD68-positive area as a percentage of plaque lesion area. *****p*<0.0001, unpaired two-tailed Student's t-test. All data represent the mean ± SEM.

Figure 6. Endothelial deficiency of ATGL upregulates endoplasmic reticulum (ER) stress and pro-inflammatory gene expression in aortic endothelial cells following a short-term atherogenic diet. A) Uniform manifold approximation and projection (UMAP) representation of aligned gene expression data in single cells extracted from aortas of control and *Atgl* ECKO mice injected with rAAV8-*mPcsk9* and fed an atherogenic diet for 4-weeks. **B)** Heat map depicting gene expression patterns of known markers of fibroblasts, smooth muscle cells (SMCs), red blood cells (RBCs), endothelial cells (ECs) and CD45+ immune cells. **C)** Volcano plot depicting differential gene expression patterns in the endothelial cell cluster between *Atgl* ECKO + *mPcsk9* compared to control + *mPcsk9* mice and expressed as log2 Fold Change (FC) along the y-axis the percent of cell expression of individual genes along the x-axis. **D)** Pathway enrichment of upregulated differentially expressed genes in the endothelial cell cluster between *Atgl* ECKO + *mPcsk9* compared to control + *mPcsk9* mice and expressed as the log[–P] and analyzed by Ingenuity Pathway Analysis. **E)** Expression profiles in the EC cluster showing the relative expression of the endoplasmic reticulum stress genes, *Hspa5*, *Ddit3*, and *Atf4* and the pro-inflammatory gene, *Vcam1*, between control + *mPcsk9* and *Atgl* ECKO + *mPcsk9* mice**. F)** Quantification of mean fluorescent intensity (MFI) of PE-VCAM1 in aortic endothelial cells ($CD31^+/CD45^-$) between control + *mPcsk9* and *Atgl* ECKO + *mPcsk9*. (n=7 replicates/group). **p*<0.05, unpaired two-tailed Student's t-test.

Graphical Abstract. **Loss of endothelial-specific ATGL accelerates atherosclerosis progression through reduction of nitric oxide signaling and endoplasmic reticulum stress induced inflammation.** Lipoprotein lipase (LPL) on the luminal surface of EC hydrolyzes circulating triglyceride rich lipoproteins (chylomicron [CM], very-low density lipoprotein [VLDL])

and releases of free fatty acid (FFA) for uptake by the endothelium though passive traversing of the plasma membrane (flip-flop) or facilitated uptake by receptor mediated and/or vectorial transport pathways. FFA bound to albumin in circulation is also taken up by the endothelium through similar mechanisms. Once inside the EC, FFA can be esterified into lipid droplets (LD) in the endoplasmic reticulum- a process that is largely dependent on diacylglycerol O-acyltransferase 1 (DGAT1). Conversely, LD are hydrolyzed by ATGL (adipose triglyceride lipase) to liberate FFA for mitochondrial oxidation and/or for parenchymal delivery. Deletion of the ATGL in the endothelium leads to neutral lipid accumulation in vessels and impairs large vessel endothelial dependent vascular tone and nitric oxide synthesis to promote endothelial dysfunction in mice. Mechanistically, the loss of ATGL leads to endoplasmic reticulum stress-induced endothelial activation, thereby contributing to EC dysfunction. Consistently, deletion of endothelial ATGL markedly increases lesion size in a model of atherosclerosis.

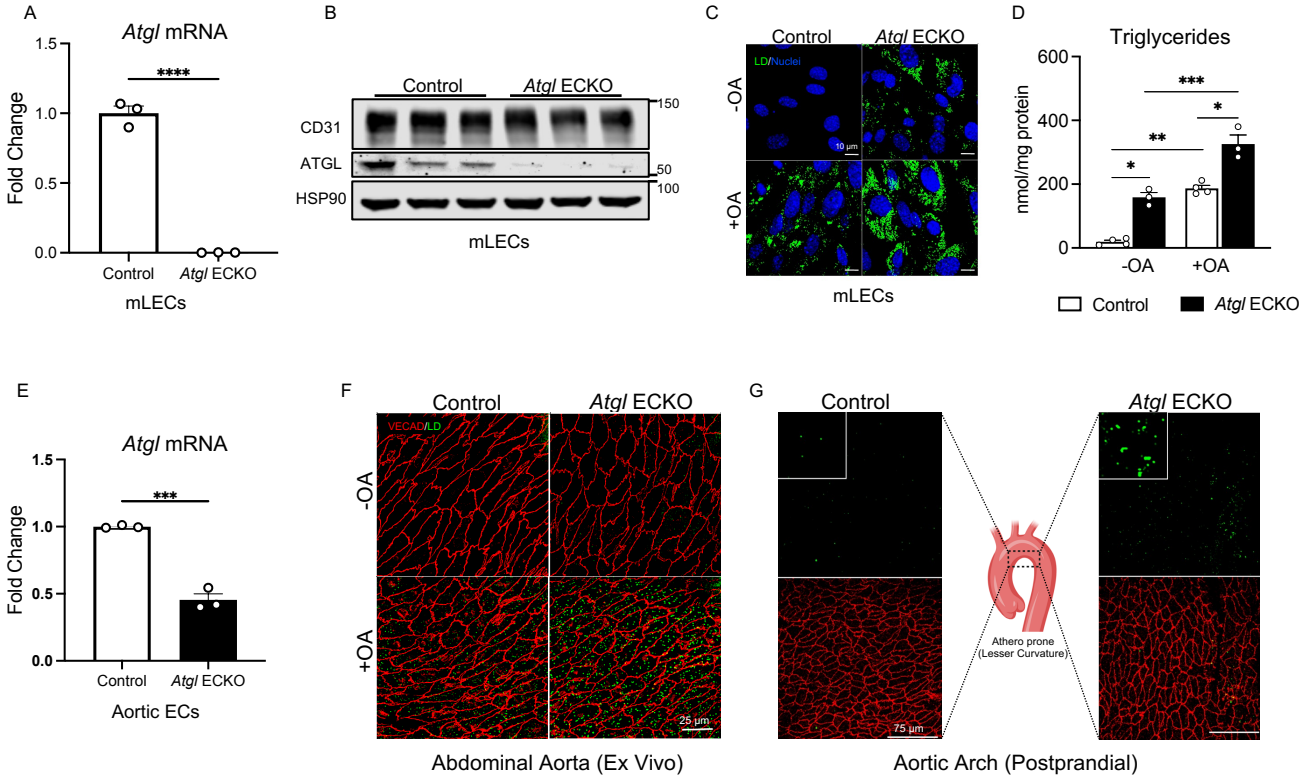
A
Atgl mRNA
Fold Change
1.5
1.0
0.5
0.0
****
Control
Atgl ECKO
mLECs
B
Control
Atgl ECKO
CD31
ATGL
HSP90
150
50
100
mLECs
C
Control
Atgl ECKO
LD/Nuclei
-OA
+OA
10 μm
mLECs
D
Triglycerides
nmol/mg protein
600
400
200
0
***
**
*
*
-OA
+OA
Control
Atgl ECKO
E
Atgl mRNA
Fold Change
1.5
1.0
0.5
0.0
***
Control
Atgl ECKO
Aortic ECs
F
Control
Atgl ECKO
VECAD/LD
-OA
+OA
25 μm
Abdominal Aorta (Ex Vivo)
G
Control
Atgl ECKO
Athero prone
(Lesser Curvature)
75 μm
Aortic Arch (Postprandial)

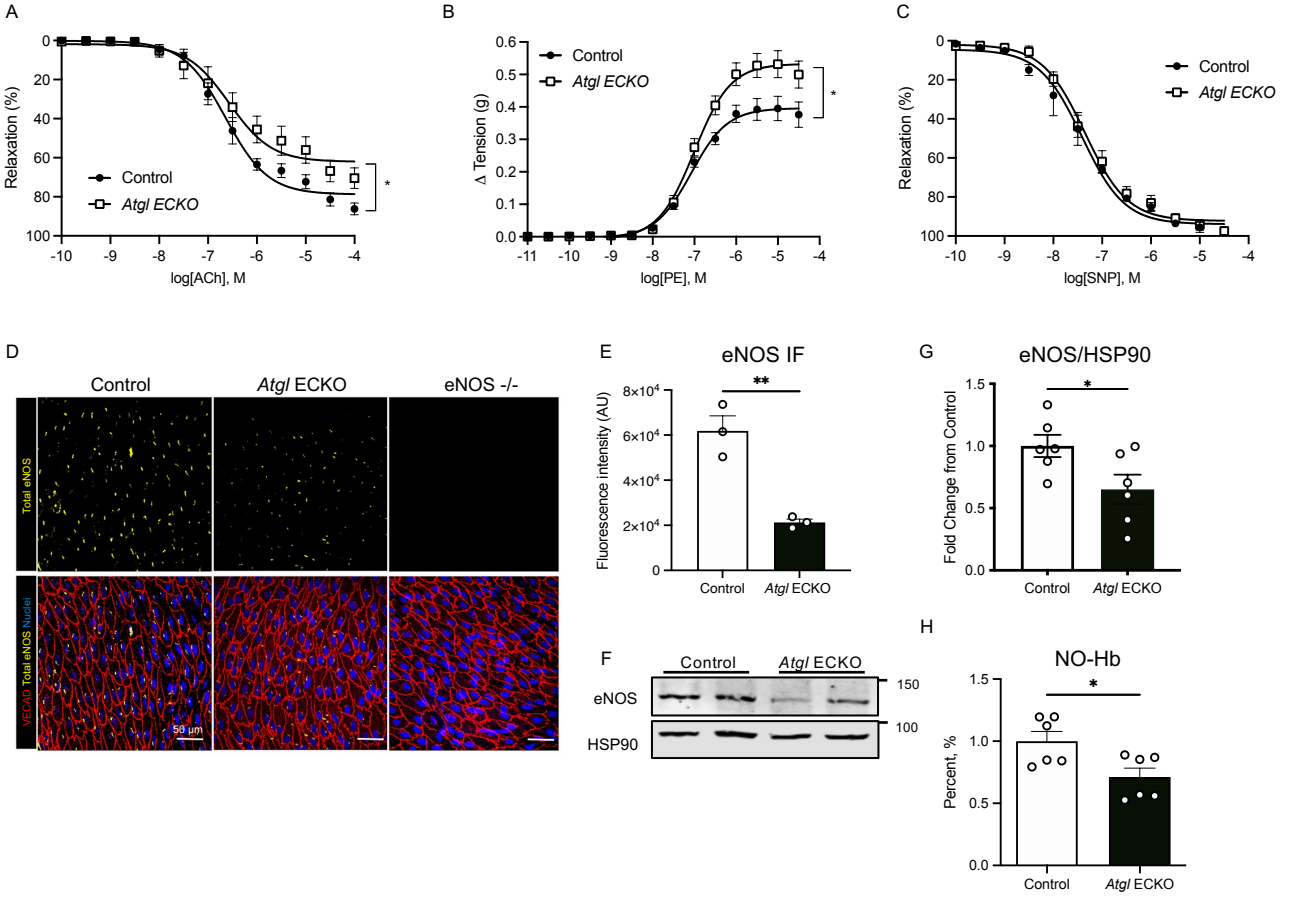
A
Relaxation (%)
log[ACh], M
Control
Atgl ECKO
*
B
Δ Tension (g)
log[PE], M
Control
Atgl ECKO
*
C
Relaxation (%)
log[SNP], M
Control
Atgl ECKO
D
Control
Atgl ECKO
eNOS -/-
Total eNOS
VECAD Total eNOS Nuclei
50 μm
E
eNOS IF
Fluorescence intensity (AU)
**
Control
Atgl ECKO
F
Control
Atgl ECKO
eNOS
HSP90
150
100
G
eNOS/HSP90
Fold Change from Control
*
Control
Atgl ECKO
H
NO-Hb
Percent, %
*
Control
Atgl ECKO

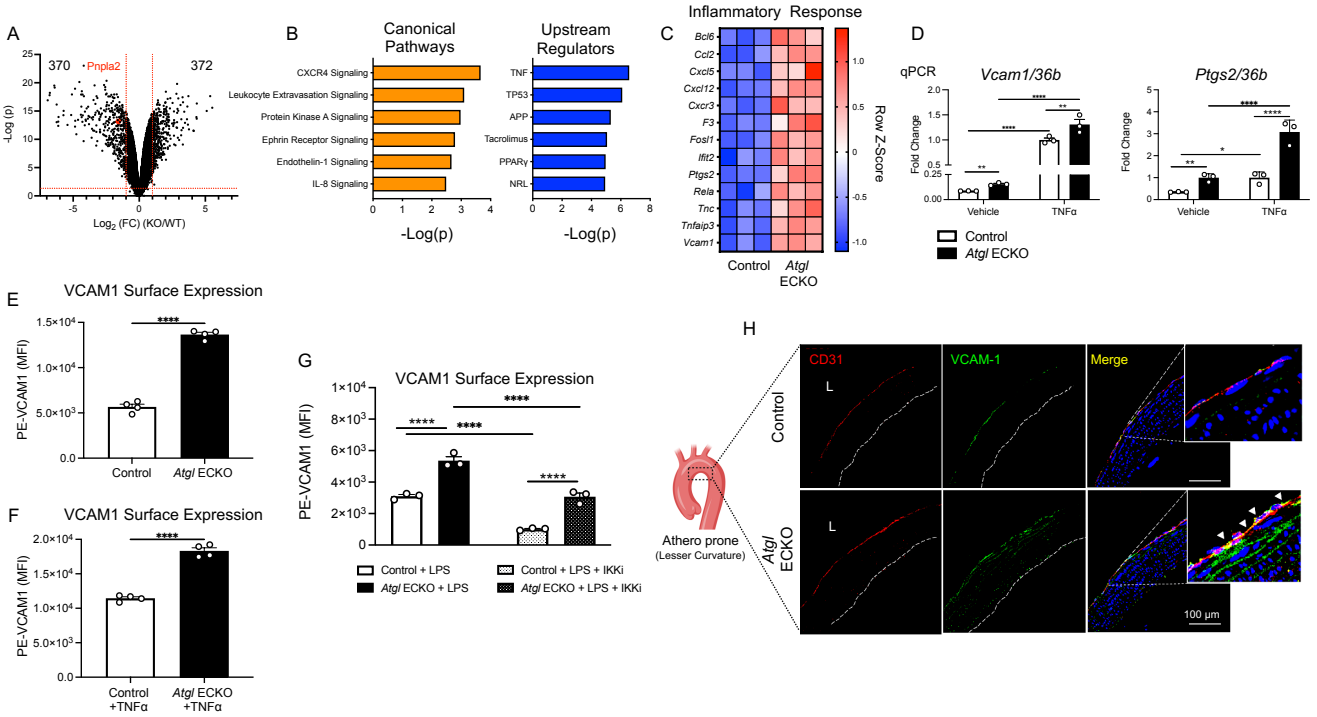
A
370
Pnpla2
372
-Log (p)
Log2 (FC) (KO/WT)
B
Canonical Pathways
CXCR4 Signaling
Leukocyte Extravasation Signaling
Protein Kinase A Signaling
Ephrin Receptor Signaling
Endothelin-1 Signaling
IL-8 Signaling
-Log(p)
Upstream Regulators
TNF
TP53
APP
Tacrolimus
PPARγ
NRL
-Log(p)
C
Inflammatory Response
Bcl6
Ccl2
Cxcl5
Cxcl12
Cxcr3
F3
Fosl1
Ifit2
Ptgs2
Rela
Tnc
Tnfaip3
Vcam1
Row Z-Score
Control
Atgl ECKO
D
qPCR
Vcam1/36b
Fold Change
Vehicle
TNFα
Control
Atgl ECKO
Ptgs2/36b
Fold Change
Vehicle
TNFα
E
VCAM1 Surface Expression
PE-VCAM1 (MFI)
Control
Atgl ECKO
F
VCAM1 Surface Expression
PE-VCAM1 (MFI)
Control +TNFα
Atgl ECKO +TNFα
G
VCAM1 Surface Expression
PE-VCAM1 (MFI)
Control + LPS
Atgl ECKO + LPS
Control + LPS + IKKi
Atgl ECKO + LPS + IKKi
H
Athero prone
(Lesser Curvature)
Control
Atgl ECKO
CD31
VCAM-1
Merge
L
100 μm

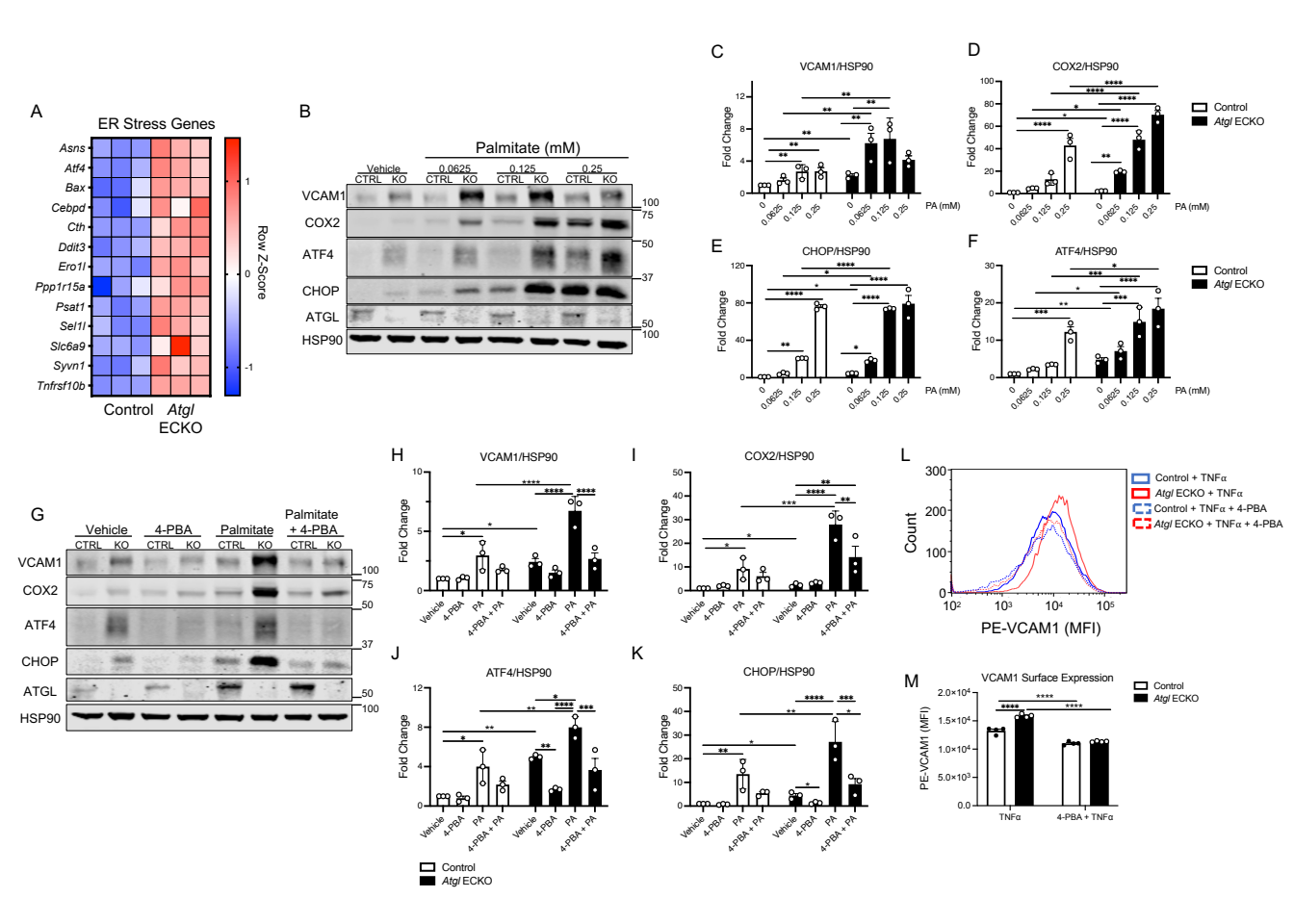
A
ER Stress Genes
Asns
Atf4
Bax
Cebpd
Cth
Ddit3
Ero1l
Ppp1r15a
Psat1
Sel1l
Slc6a9
Syvn1
Tnfrsf10b
Row Z-Score
Control
Atgl ECKO
B
Palmitate (mM)
Vehicle
0.0625
0.125
0.25
CTRL KO
VCAM1
COX2
ATF4
CHOP
ATGL
HSP90
C
VCAM1/HSP90
D
COX2/HSP90
E
CHOP/HSP90
F
ATF4/HSP90
Fold Change
PA (mM)
Control
Atgl ECKO
G
Vehicle
4-PBA
Palmitate
Palmitate + 4-PBA
H
I
J
K
L
Control + TNFα
Atgl ECKO + TNFα
Control + TNFα + 4-PBA
Atgl ECKO + TNFα + 4-PBA
Count
PE-VCAM1 (MFI)
M
VCAM1 Surface Expression
TNFα
4-PBA + TNFα

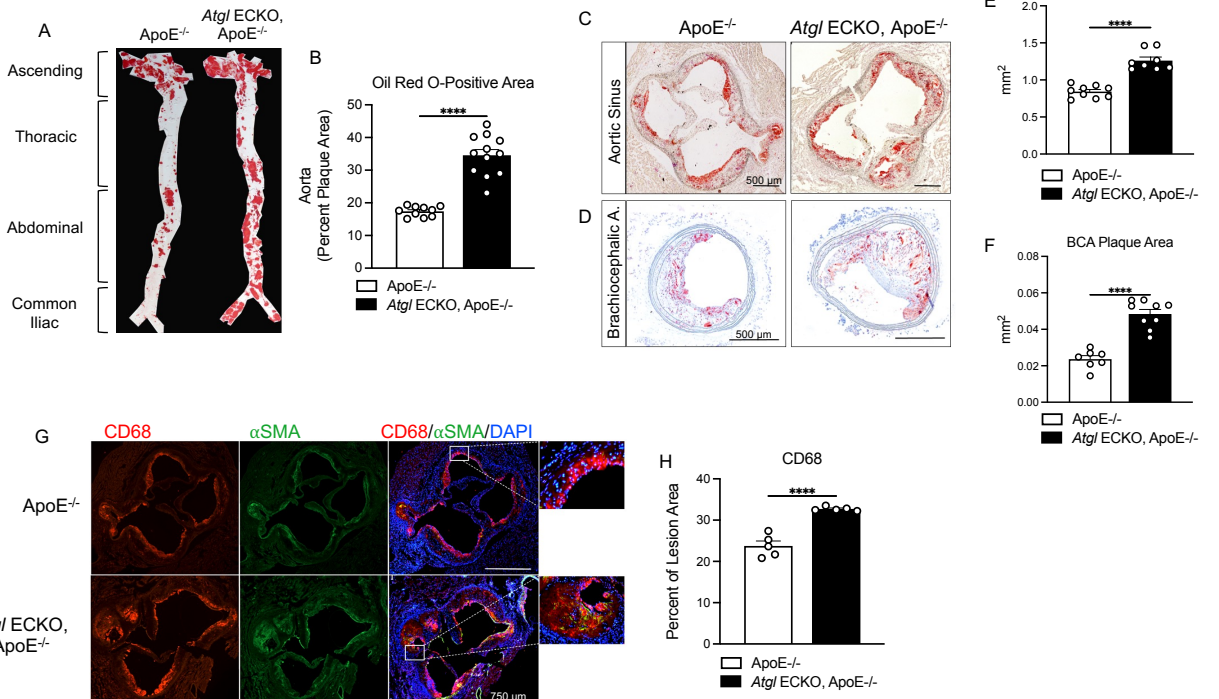
A
ApoE-/-
Atgl ECKO, ApoE-/-
Ascending
Thoracic
Abdominal
Common Iliac
B
Oil Red O-Positive Area
Aorta (Percent Plaque Area)
****
ApoE-/-
Atgl ECKO, ApoE-/-
C
ApoE-/-
Atgl ECKO, ApoE-/-
Aortic Sinus
500 μm
D
Brachiocephalic A.
500 μm
E
Aortic Sinus Plaque Area
mm2
****
ApoE-/-
Atgl ECKO, ApoE-/-
F
BCA Plaque Area
mm2
****
ApoE-/-
Atgl ECKO, ApoE-/-
G
CD68
αSMA
CD68/αSMA/DAPI
ApoE-/-
Atgl ECKO, ApoE-/-
750 μm
H
CD68
Percent of Lesion Area
****
ApoE-/-
Atgl ECKO, ApoE-/-

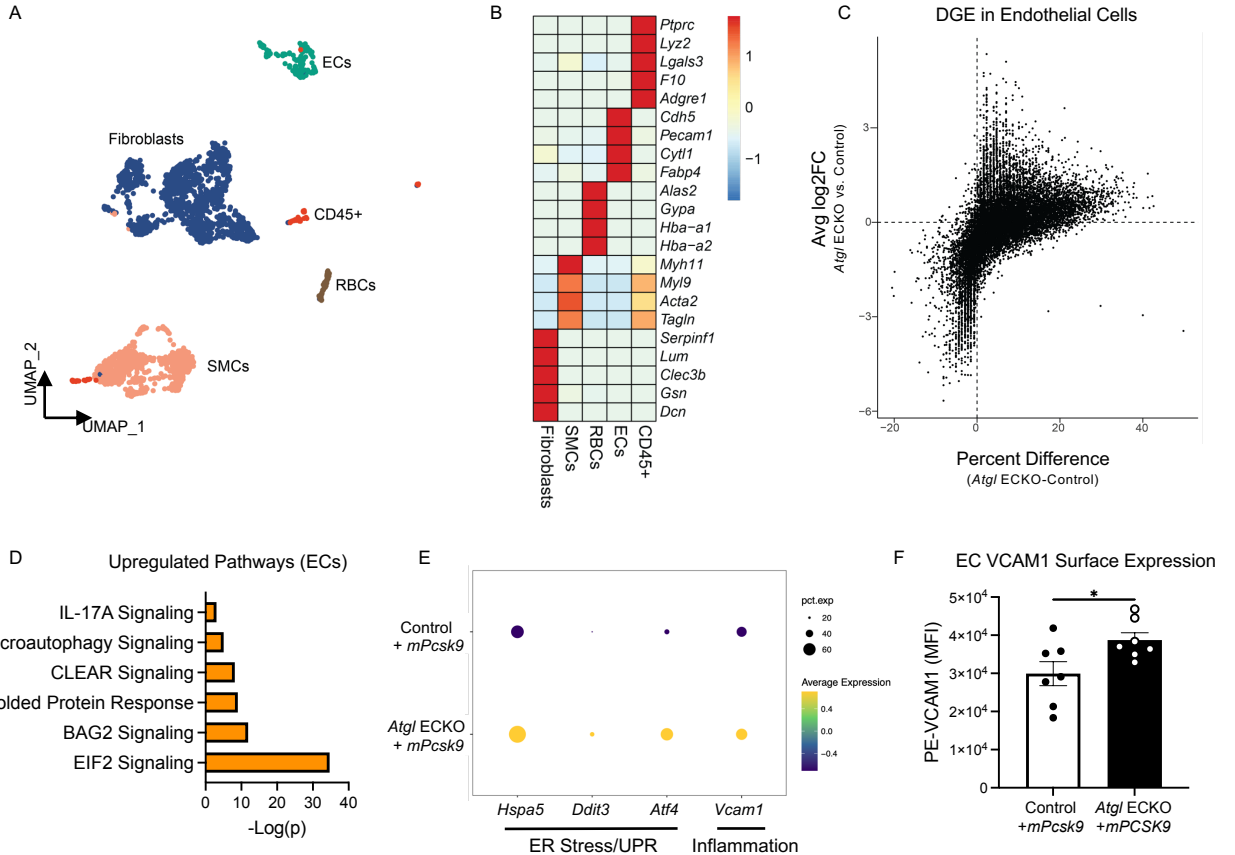
A
ECs
Fibroblasts
CD45+
RBCs
SMCs
UMAP_2
UMAP_1
B
Ptprc
Lyz2
Lgals3
F10
Adgre1
Cdh5
Pecam1
Cytl1
Fabp4
Alas2
Gypa
Hba−a1
Hba−a2
Myh11
Myl9
Acta2
Tagln
Serpinf1
Lum
Clec3b
Gsn
Dcn
1
0
−1
Fibroblasts
SMCs
RBCs
ECs
CD45+
C
DGE in Endothelial Cells
Avg log2FC
Atgl ECKO vs. Control)
3
0
−3
−6
−20
0
20
40
Percent Difference
(Atgl ECKO-Control)
D
Upregulated Pathways (ECs)
IL-17A Signaling
Microautophagy Signaling
CLEAR Signaling
Unfolded Protein Response
BAG2 Signaling
EIF2 Signaling
0
10
20
30
40
-Log(p)
E
Control
+ mPcsk9
Atgl ECKO
+ mPcsk9
Hspa5
Ddit3
Atf4
Vcam1
ER Stress/UPR
Inflammation
pct.exp
20
40
60
Average Expression
0.4
0.0
−0.4
F
EC VCAM1 Surface Expression
5×10^4
4×10^4
3×10^4
2×10^4
1×10^4
0
PE-VCAM1 (MFI)
*
Control
+mPcsk9
Atgl ECKO
+mPCSK9

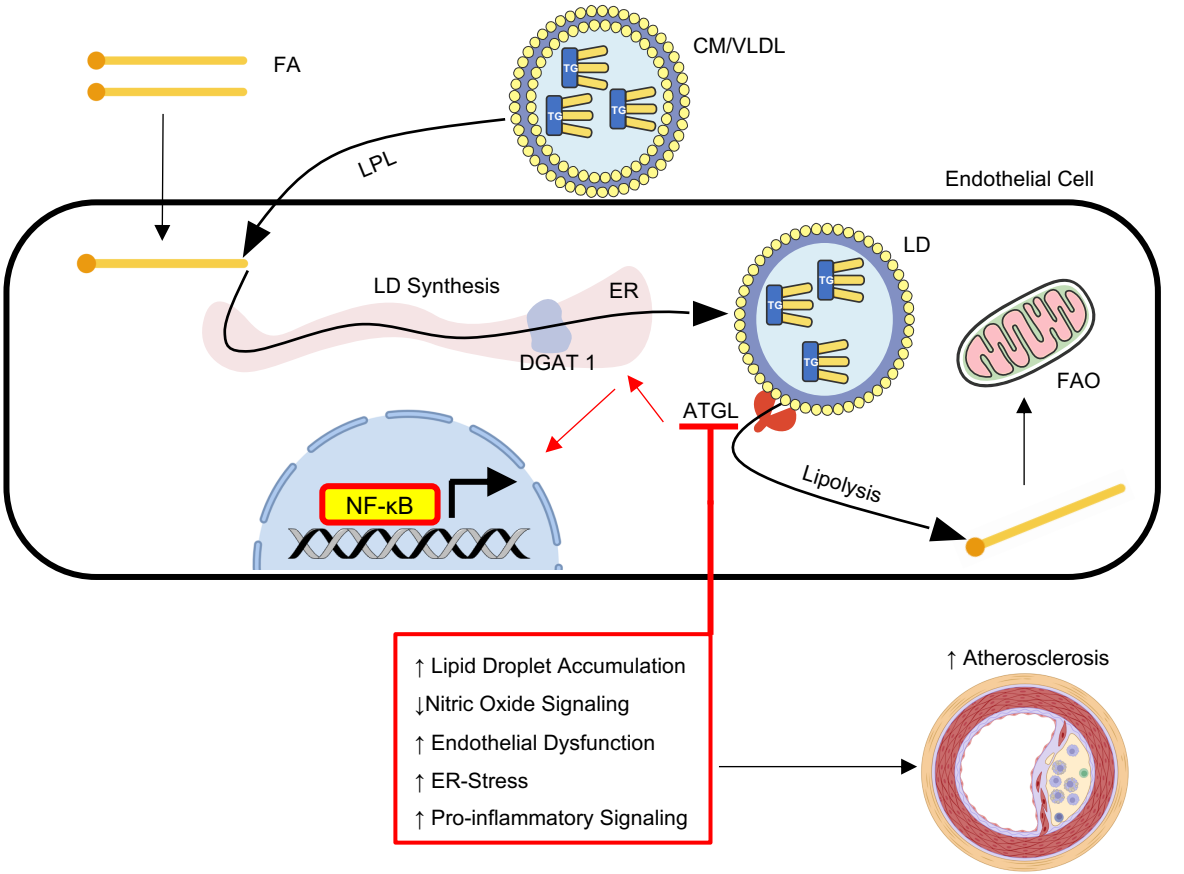
FA
CM/VLDL
TG
TG
TG
LPL
Endothelial Cell
LD
LD Synthesis
ER
DGAT 1
TG
TG
TG
FAO
ATGL
NF-κB
Lipolysis
↑ Lipid Droplet Accumulation
↓Nitric Oxide Signaling
↑ Endothelial Dysfunction
↑ ER-Stress
↑ Pro-inflammatory Signaling
↑ Atherosclerosis

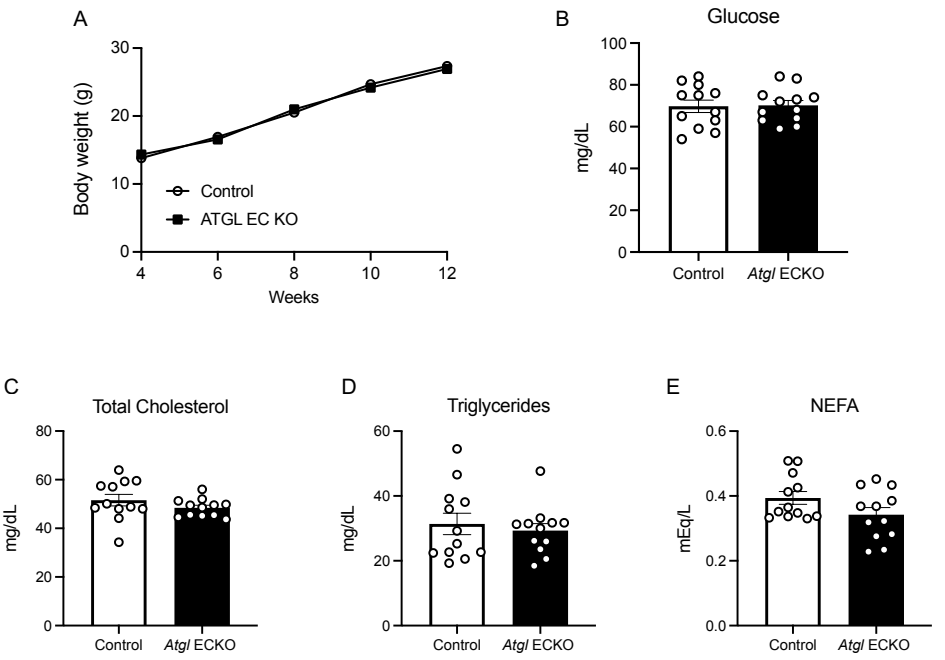
A
Body weight (g)
30
20
10
0
4
6
8
10
12
Weeks
Control
ATGL EC KO
B
Glucose
mg/dL
100
80
60
40
20
0
Control
Atgl ECKO
C
Total Cholesterol
mg/dL
80
60
40
20
0
Control
Atgl ECKO
D
Triglycerides
mg/dL
60
40
20
0
Control
Atgl ECKO
E
NEFA
mEq/L
0.6
0.4
0.2
0.0
Control
Atgl ECKO

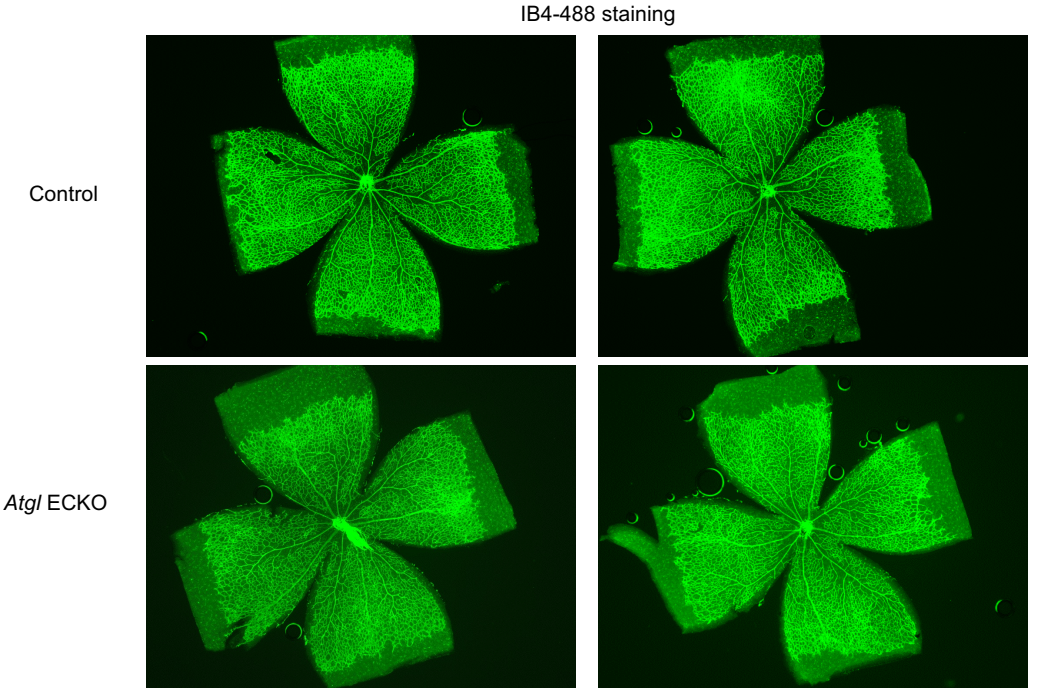
IB4-488 staining
Control
Atgl ECKO

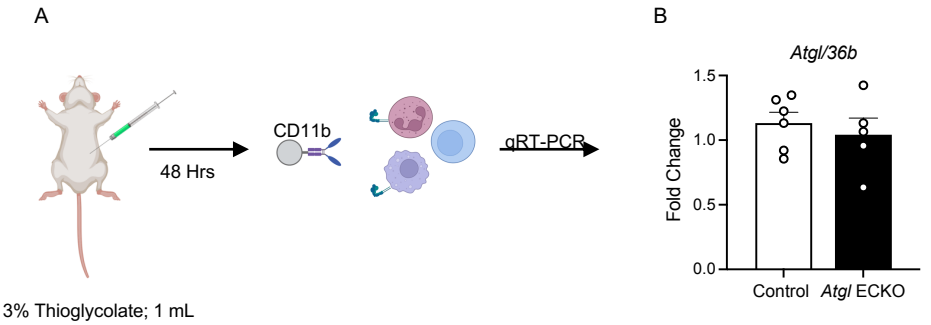
A
48 Hrs
CD11b
qRT-PCR
3% Thioglycolate; 1 mL
B
Atgl/36b
Fold Change
1.5
1.0
0.5
0.0
Control
Atgl ECKO

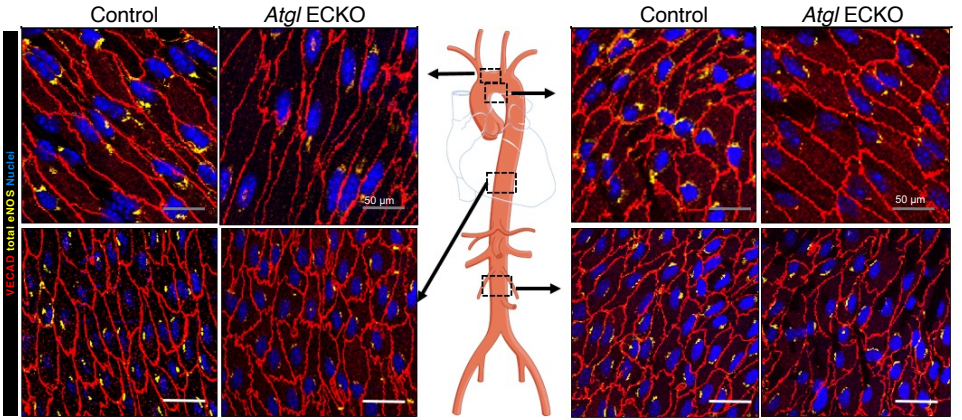
Control
Atgl ECKO
Control
Atgl ECKO
VECAD total eNOS Nuclei
50 µm
50 µm

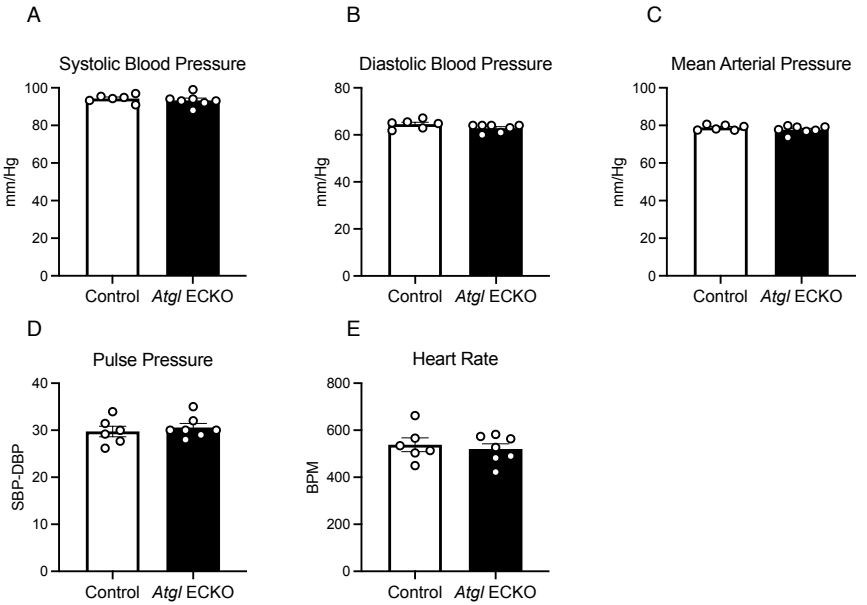
A
Systolic Blood Pressure
mm/Hg
100
80
60
40
20
0
Control
Atgl ECKO
B
Diastolic Blood Pressure
mm/Hg
80
60
40
20
0
Control
Atgl ECKO
C
Mean Arterial Pressure
mm/Hg
100
80
60
40
20
0
Control
Atgl ECKO
D
Pulse Pressure
SBP-DBP
40
30
20
10
0
Control
Atgl ECKO
E
Heart Rate
BPM
800
600
400
200
0
Control
Atgl ECKO

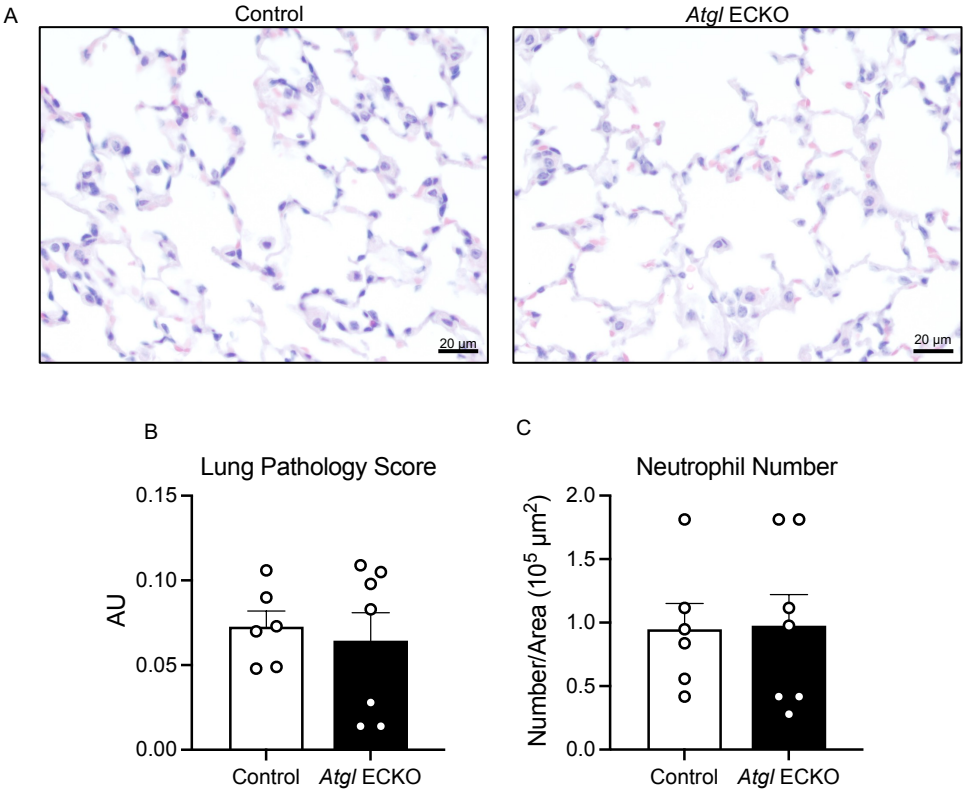
A
Control
Atgl ECKO
20 μm
20 μm
B
Lung Pathology Score
AU
0.15
0.10
0.05
0.00
Control
Atgl ECKO
C
Neutrophil Number
Number/Area (10^5 μm^2)
2.0
1.5
1.0
0.5
0.0
Control
Atgl ECKO

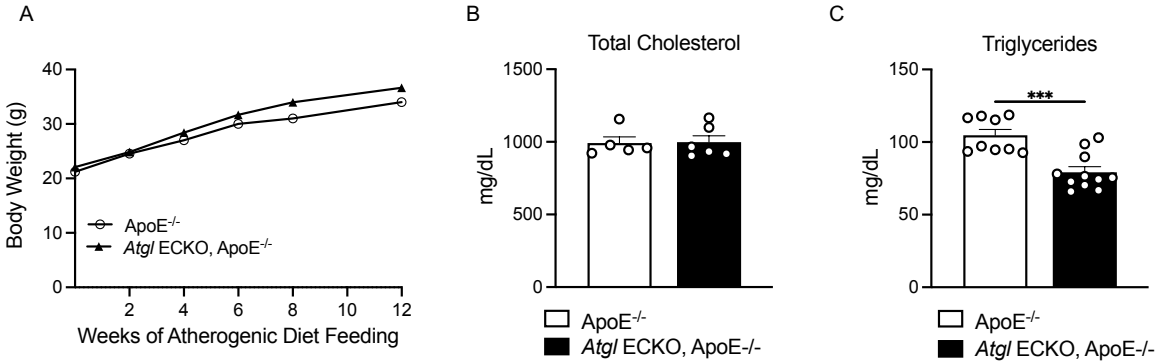
A
Body Weight (g)
40
30
20
10
0
2
4
6
8
10
12
Weeks of Atherogenic Diet Feeding
ApoE-/-
Atgl ECKO, ApoE-/-
B
Total Cholesterol
mg/dL
1500
1000
500
0
ApoE-/-
Atgl ECKO, ApoE-/-
C
Triglycerides
mg/dL
150
100
50
0
***
ApoE-/-
Atgl ECKO, ApoE-/-

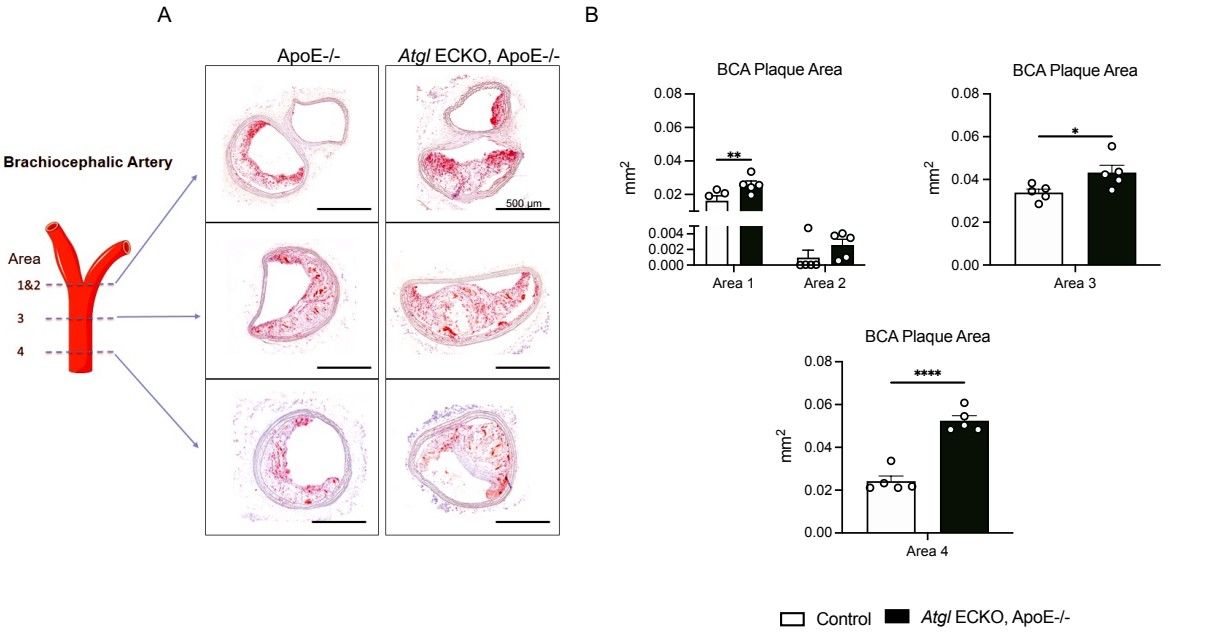
A
ApoE-/-
Atgl ECKO, ApoE-/-
Brachiocephalic Artery
Area
1&2
3
4
500 μm
B
BCA Plaque Area
mm2
0.08
0.06
0.04
0.02
0.004
0.002
0.000
**
Area 1
Area 2
BCA Plaque Area
0.08
0.06
0.04
0.02
0.00
*
Area 3
BCA Plaque Area
0.08
0.06
0.04
0.02
0.00
****
Area 4
Control
Atgl ECKO, ApoE-/-

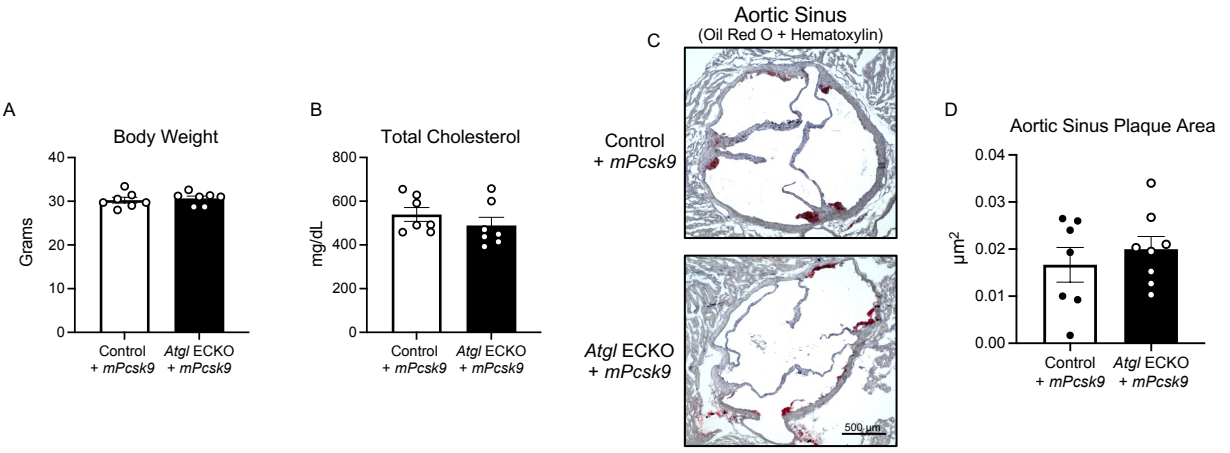
A
Body Weight
Grams
40
30
20
10
0
Control
+ mPcsk9
Atgl ECKO
+ mPcsk9
B
Total Cholesterol
mg/dL
800
600
400
200
0
Control
+ mPcsk9
Atgl ECKO
+ mPcsk9
C
Aortic Sinus
(Oil Red O + Hematoxylin)
Control
+ mPcsk9
Atgl ECKO
+ mPcsk9
500 µm
D
Aortic Sinus Plaque Area
µm2
0.04
0.03
0.02
0.01
0.00
Control
+ mPcsk9
Atgl ECKO
+ mPcsk9